UNIVERSIDAD DE INVESTIGACIÓN DE TECNOLOGÍA EXPERIMENTAL YACHAY

Escuela de Ciencias Físicas y Nanotecnología

TÍTULO: Conductive/Luminescence Hybrid Compounds Based on Chitosan Doped with LiClO$_4$ and ZnO

Trabajo de integración curricular presentado como requisito para la obtención del título de Ingeniería en Nanotecnología

Autor:

Gurumendi Sánchez Marlon Patricio

Tutor:

Ph.D González Vásquez Gema

Urcuquí, agosto 2019

SECRETARÍA GENERAL
(Vicerrectorado Académico/Cancillería)
ESCUELA DE CIENCIAS FÍSICAS Y NANOTECNOLOGÍA
CARRERA DE NANOTECNOLOGÍA
ACTA DE DEFENSA No. UITEY-PHY-2019-00002-AD

En la ciudad de San Miguel de Urcuquí, Provincia de Imbabura, a los 20 días del mes de agosto de 2019, a las 08:30 horas, en el Aula Sala Capitular de la Universidad de Investigación de Tecnología Experimental Yachay y ante el Tribunal Calificador, integrado por los docentes:

Presidente Tribunal de Defensa	BRICEÑO ARAUJO, SARAH ELISA
Miembro No Tutor	JANI MONA
Tutor	GONZALEZ VASQUEZ, GEMA

Se presenta el(la) señor(ita) estudiante **GURUMENDI SANCHEZ, MARLON PATRICIO**, con cédula de identidad No. **0923017248**, de la **ESCUELA DE CIENCIAS FÍSICAS Y NANOTECNOLOGÍA**, de la Carrera de **NANOTECNOLOGÍA**, aprobada por el Consejo de Educación Superior (CES), mediante Resolución **RPC-SO-13-No.156-2015**, con el objeto de rendir la sustentación de su trabajo de titulación denominado: **Conductive/Luminescence Hybrid Compounds Based on Chitosan Doped with LiClO4 and ZnO**, previa a la obtención del título de **INGENIERO/A EN NANOTECNOLOGÍA**.

El citado trabajo de titulación, fue debidamente aprobado por el(los) docente(s):

Tutor	GONZALEZ VASQUEZ, GEMA

Y recibió las observaciones de los otros miembros del Tribunal Calificador, las mismas que han sido incorporadas por el(la) estudiante.

Previamente cumplidos los requisitos legales y reglamentarios, el trabajo de titulación fue sustentado por el(la) estudiante y examinado por los miembros del Tribunal Calificador. Escuchada la sustentación del trabajo de titulación, que integró la exposición de el(la) estudiante sobre el contenido de la misma y las preguntas formuladas por los miembros del Tribunal, se califica la sustentación del trabajo de titulación con las siguientes calificaciones:

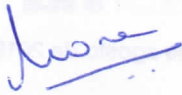| Tipo	Docente	Calificación
Tutor	GONZALEZ VASQUEZ, GEMA	10,0
Presidente Tribunal De Defensa	BRICEÑO ARAUJO, SARAH ELISA	9,3
Miembro Tribunal De Defensa	JANI MONA	9,0

Lo que da un promedio de: **9.4 (Nueve punto Cuatro)**, sobre 10 (diez), equivalente a: **APROBADO**

Para constancia de lo actuado, firman los miembros del Tribunal Calificador, el/la estudiante y el/la secretario ad-hoc.

GURUMENDI SANCHEZ, MARLON PATRICIO
Estudiante
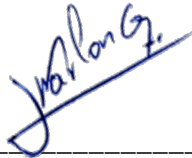
BRICEÑO ARAUJO, SARAH ELISA
Presidente Tribunal de Defensa

GONZALEZ VASQUEZ, GEMA
Tutor

JANI MONA
Miembro No Tutor

CIFUENTES TAFUR, EVELYN CAROLINA
Secretario Ad-hoc

AUTORÍA

Yo, **MARLON PATRICIO GURUMENDI SÁNCHEZ**, con cédula de identidad 0923017248, declaro que las ideas, juicios, valoraciones, interpretaciones, consultas bibliográficas, definiciones y conceptualizaciones expuestas en el presente trabajo; así cómo, los procedimientos y herramientas utilizadas en la investigación, son de absoluta responsabilidad de el/la autora (a) del trabajo de integración curricular. Así mismo, me acojo a los reglamentos internos de la Universidad de Investigación de Tecnología Experimental Yachay.

Urcuquí, agosto 2019.

_____

Marlon Patricio Gurumendi Sánchez
CI: 0923017248

AUTORIZACIÓN DE PUBLICACIÓN

Yo, **MARLON PATRICIO GURUMENDI SÁNCHEZ,** con cédula de identidad 0923017248, cedo a la Universidad de Tecnología Experimental Yachay, los derechos de publicación de la presente obra, sin que deba haber un reconocimiento económico por este concepto. Declaro además que el texto del presente trabajo de titulación no podrá ser cedido a ninguna empresa editorial para su publicación u otros fines, sin contar previamente con la autorización escrita de la Universidad.

Asimismo, autorizo a la Universidad que realice la digitalización y publicación de este trabajo de integración curricular en el repositorio virtual, de conformidad a lo dispuesto en el Art. 144 de la Ley Orgánica de Educación Superior

Urcuquí, agosto 2019.

_____
Marlon Patricio Gurumendi Sánchez
CI: 0923017248

Dedicatoria

Me gustaría dedicar este trabajo a mi mamá y papá por su apoyo, confianza y aliento, y por ser el pilar fundamental de mi educación académica al brindarme la oportunidad de estudiar en la universidad Yachay Tech. A mis hermanos Bryan y Jonathan, cuya inspiración y aliento hicieron posible este trabajo. A mi querida esposa, por su amor, compañía y paciencia desde el momento en que entró en mi vida. No puedo olvidar a la Dra. Gema González por su apoyo y conocimiento. Además, a la Dra. Floralba López por su apoyo y ayuda. Una dedicación especial a mi hijo, quien amo con todo mi corazón.

Marlon Patricio Gurumendi Sánchez

Agradecimiento

Resumen

El quitosano (CS) es un biopolimérico natural altamente biocompatible que se produce en países con grandes camaroneras, como Ecuador. La ventaja de CS es que, debido a su estructura, se puede combinar con una variedad de compuestos para obtener diferentes propiedades, para aplicaciones específicas. Entre ellos, el diseño de nuevos dispositivos electrónicos tales como supercondensadores, sistemas de bioimagen, diodos emisores de luz orgánicos (OLED) desde un polímero natural siguiendo una síntesis aplicando química verde es un desafío digno de emprender. Aunque se ha informado poco sobre el uso de CS para estas aplicaciones, se ha demostrado que la adición de ciertas sales aumenta sus propiedades eléctricas. Por lo tanto, el objetivo del presente trabajo es modificar CS para mejorar sus propiedades eléctricas y de luminiscencia con el fin de obtener nuevas aplicaciones en dispositivos biomédicos y optoelectrónicos. Se prepararon películas delgadas híbridas CS que contenían iones de ZnO y Li usando el método de fundición de solución. Se agrega litio para aumentar la conductividad iónica y ZnO para propiedades de luminiscencia. Para seguir los cambios estructurales en la película de quitosano se realizaron diversas técnicas de caracterización. Difracción de rayos X (XRD), espectroscopía infrarroja por transformada de Fourier (FTIR), microscopía electrónica de barrido (SEM) y UV-Visible. Además, la conductividad iónica de las diferentes soluciones se midió mediante impedancia compleja, y también se realizaron mediciones de fotoluminiscencia. La adición de Li se observó muy claramente en el FTIR con la presencia de la banda de vibración a 623 cm^{-1} hasta el 10%. La DRX mostró los picos característicos de quitosano a 11.94 y 18.70°. La adición de Li en alta concentración (hasta 40%) indujo la amorfización en la membrana de quitosano. La conductividad iónica de las películas de polímero aumentó con las concentraciones de $LiClO_4$. El análisis UV-Vis reveló que la concentración de $LiClO_4$ afecta la banda de absorción. La fotoluminiscencia de quitosano se observó a 497 nm y su intensidad aumentó ajustando la concentración de $LiClO_4$. Por lo tanto, estos resultados sugieren que las películas de quitosano dopadas con iones Li y Zn tienen un potencial como electrolito polimérico para diferentes aplicaciones.

Palabras Clave:

Abstract

Chitosan (CS) is a natural biopolymer highly biocompatible produce in countries with large shrimp farms, like Ecuador. The advantage of CS is that due to its structure it can be combined with a variety of compounds to obtain different properties, for specific applications. Among them, the design of electronic devices of new electronic devices such as supercapacitors, systems for bioimaging, organic emitting diode (OLED) from a natural polymer following a green chemistry synthesis is a challenge worthy to undertake. Although, little work has been reported on the use of CS for these applications, however the addition of certain salts has been proved to increase its electrical properties. Therefore, the objective of the present work is to modify CS to improve its electrical and luminescence properties in order to obtain new applications in biomedical and opto-electronic devices. CS hybrid thin films containing ZnO and Li ions were prepared by using solution casting method. Lithium is added to increase the ionic conductivity and ZnO for luminescence properties. To follow the structural changes in the chitosan film various characterization techniques were performed. X-ray diffraction (XRD), Fourier Transform Infrared spectroscopy (FTIR), Scanning Electron Microscopy (SEM), and UV-Visible. Additionally, the ionic conductivity of the different solutions was measured by Electrochemical Impedance Spectroscopy (EIS), and photoluminescence measurements were also carried out. The addition of Li was very clearly observed in the FTIR with the presence of the vibration band at 623 cm^{-1} up to 10%. XRD showed the characteristic peaks of chitosan at 11.94 and 18.70°. The addition of Li in high concentration (up to 40%) induced amorphization in the chitosan membrane. The ionic conductivity of the polymer films increased with $LiClO_4$ concentrations. UV-Vis analysis revealed that the $LiClO_4$ concentration affect the absorption band. The chitosan photoluminescence was observed at 497 nm and its intensity increased by tuning the $LiClO_4$ concentration. Therefore, these results suggested that the chitosan films doped with Li and Zn ions have a potential as a polymer electrolyte for different applications.

Key Words:

Contents

List of Figures

List of Tables

Chapter 1

Introduction

The polymer stated to use massively in 1950, and since then they were used in more applications, now the volume of polymer used in our world is higher than metal. Thus, the development of potential materials that are friendly to the environment with low toxicity, biocompatibility, sustainability and profitability have been increasing over the years. The blending of polymer and salt is an important process to create polymer electrolytes that provide ions as charge carriers into a polymer matrix. Different solid polymers electrolytes have been studied, such as, chitosan thin film due to its wide use in protonic batteries[1], lithium rechargeable batteries[2], secondary cells of lithium[3], supercapacitors[4] and fuel cells[5]. Chitosan is a polysaccharide derived from chitin, which is extracted from shells of crustaceans. It has advantages such as biodegradability, biocompatibility, non-toxicity and is excellent film-forming. On the other hand, the most common salts for preparing solid polymer electrolytes are lithium perchlorate $(LiClO_4)$[4] and lithium triflate $(LiCF_3SO_3)$[3] because the lithium ion is the lightest metal and could give largest energy content. Finding constant ways to improve the properties of different materials, as for example, conductivity, luminescence, strength, among others, have become a challenge for scientists. Hence, ways to discover low cost manufacturing methods and materials with low metal content to avoid damages in the environment are looked for with positive impacts on living conditions within society. This approach has become an important key for researchers. Extensive research has shown that the polysaccharide chitosan can disperse inorganic salts in sufficient quantities into its matrix to form new hybrid material which differs in its properties compared to pure state. Thus, chitosan enables to incorporate ions to its matrix due to its amorphous phase, and nanoparticles because of its adhesive and sorption properties can retain NPs onto its surface producing advanced materials. On the other side, luminescence-based advanced functional materials attracted considerable attention in recent years. Therefore, adding nanoparticles with luminescence properties such as ZnO can result in solid electrolytes with these properties. This project proposes the doping of chitosan using $LiClO_4$ and ZnO to study the conductivity and luminescence properties.

1.1   Problem Statement

The use of chitosan for the development of new devices is an alternative contribution to the design of product and processes that minimize the use and generation of hazardous substances (green chemistry). Additionally, this polymer comes from shrimp waste subproduct that can be valorized. In Ecuador there is the exploitation of the shrimp resource, so finding applications to add value to the chitosan is of great importance. The use of low-cost natural materials for the manufacture of electronic devices is currently of great interest. Chitosan and lithium ions are soluble in organic solvents and have already shown applicability in solid polymer electrolytes such as proton batteries[1] and supercapacitors[4].

The need to create hybrid compounds based on chitosan capable of having good properties, such as luminescence and high ionic conductivity, with possible applications in solid polymer electrolytes, such as lithium batteries, solar cells or supercapacitors is an important challenge. The addition of an ion solvating to a solid polymer forms a solid polymer electrolyte (SPE), assuring a homogenous ion distribution within the active layer[6]. Herein knowing that chitosan provides good ion solvating properties, the addition of specific ions may contribute to higher ionic conductivities in the material. Therefore, this project proposes the preparation of chitosan membranes doped with $LiClO_4$ and ZnO for potential applications in electronic devices. Furthermore, currently there are no systems reported about ZnO and $LiClO_4$ dispersed onto chitosan. Adding these two components can enhance the chitosan properties.

Based on previous research, lithium perchlorate can extend and improve the conductivity of chitosan due to the interactions between the lithium and chitosan, such as ionic interactions and chemical bonding. Also, the use of inorganic components like zinc oxide that emit light can increase luminescence in this polymer.

1.2   General and Specific Objectives

1.2.1   General Objective

The study of hybrid chitosan based compounds to improve their properties of conductivity and luminescence.

1.2.2   Specific Objectives

1. Prepare thin films of chitosan with different proportions of $LiClO_4$.

2. Prepare thin films of chitosan with ZnO.

3. Prepare thin films of hybrid chitosan/$LiClO_4$/ZnO.

4. Evaluate the prepared hybrid materials by using Electrochemical Impedance Spectroscopy, Infrared Spectroscopy, X-ray diffraction, Scanning Electron Microscopy, and Photoluminescence measurements.

5. Determine the conductivity and dielectric properties of the different materials prepared.

6. Correlate the properties to the structural characterization.

Chapter 2

Theoretical Part

2.1 Polymer Electrolytes

Polymer electrolytes are membranes which have a dissolution of salt in a polymer matrix with high molecular weight[7], i.e., they can be prepared by dissolving metal salts in polar polymer hosts. These membranes have ionic conduction property and therefore are widely used in electrochemical devices such as rechargeable batteries[8,9]. They possess interesting properties like transparency, solvent-free, light-weight, flexible, thin-firm forming ability, high ionic conductivity, easy processability and wide electrochemical windows[7,10]. Polymer electrolytes have certain advantages such as avoiding leaks, not causing internal short circuits, eliminating the use of corrosive solvents and not producing harmful gases[11]. Most polymer electrolytes have been used in solar cells, fuel cells, electrochemical sensors, electric vehicles, thin credit cards, mobile cellular phone, laptop computers, etc[7].

The most outstanding property of the polymer electrolytes is the ionic conductivity[12]. This property is related to the degree of crystallinity and the viscosity of the polymer electrolytes[13]. In the crystalline phase, the ions are difficult to move, so they have low mobility[12]. Thus, the polymer electrolytes will have low conductivity. On the other hand, when the polymer electrolyte has a lower viscosity, the ionic conductivity of the electrolyte polymer will be higher because more voids will be produced in it[14,15]. In order to prepare the polymer electrolyte, it is necessary to add a material on at least one base matrix, which may be a host polymer[7]. The most used dopant material in the preparation of many polymer electrolytes are lithium salts like lithium perchlorate[16–18], lithium tetraborate[19], lithium hexafluorophosphate[20] and lithium trifluoromethanesulfonate[21].

The preference for lithium salts is due to their cations that coordinate and solvate easily to show their character of ionic conductivity. Adding salt to the polymers causes changes in the structure and optical and thermal properties[22]. A dopant salt that has attracted attention because of its low interfacial strength is lithium perchlorate ($LiClO_4$). $LiClO_4$ is composed of a large anion and a small cation. The advantage of this salt is that a complexation can be obtained when the polymer electrolytes are prepared due to their high dissociation energy and a good solubility in most solvents[17]. Figure 2.1 shows the chemical structure of $LiClO_4$.
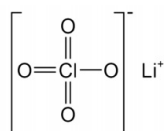
Figure 2.1: Chemical Structure of Lithium Perchlorate[7].

2.1.1   Chitosan as Electrolyte

Chitosan (CS) is a polysaccharide derived from chitin[23,24] which is the second most important natural polymer extracted from shells of crustaceans[25]. CS consists of a large number of hydroxyls and amine groups (Figure 2.2). CS has been an attractive alternative because of its high safety, low toxicity, and its physical and chemical properties[26] that can be advantageous for several technologies, including biomedical, pharmaceutical, environmental, and so on[27] related to polymers. The functional groups on the CS backbone are sufficient for dissolving organic and inorganic salts by making polyectrolyte[28–30]. CS is used as the membrane matrix owing to its good film forming and mechanical properties[31,32].
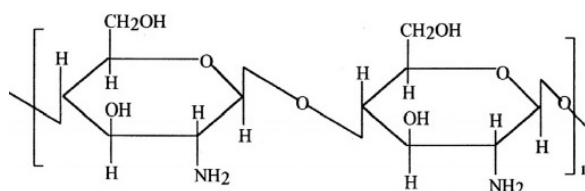
Figure 2.2: Chemical Structure of Chitosan[33].

2.1.2   Mechanisms of Chitosan Conduction

CS has a low electrical conductivity[34] which can increase by dissolving it in acetic acid[35]. When CS is swollen in acidic medium, its amino groups may be protonated or charged by leaving free ions in acidic medium[36] and thus contribute to ionic conduction in CS membrane[37]. Likewise, adding a dopant salt in the polymer matrix improves the conductivity of CS by promoting the ion migration rate through the film[38] and increasing the amorphous content[39]. Such is the case of CS membranes that have been used for active transport of chloride ions in aqueous solution[40]. These membranes put in a closed circuit, it can show a corresponding ionic conduction. Thus, CS can be used as a polymer matrix for ionic conduction[41]. For example, mixing CS with lithium nitrate changes the ionic conductivity of CS film to 10^{-4} S.cm^{-1} by demonstrating CS film can be used to fabricate polymer batteries[42]. Also, a solid polymer electrolyte was reacted by mixing CS and succinic anhydride with different ratios of lithium perchlorate. The addition of succinyl group increased the ionic conductivity values from 2.88×10^{-6} S.cm^{-1} to 3.93×10^{-4} S.cm^{-1}. Then they added 10% (w/w) lithium perchlorate, and the conductivity increased to 8.01×10^{-3} S.cm^{-1} by suggesting

that the polymer electrolyte can be used in lithium battery[43].

2.2 Luminescent Properties

Luminescence is a way of making certain materials to emit light when stimulated by a radiation source. Depending on this source, luminescence can occur in different ways such as electroluminescence or photoluminescence[44]. In general, when the material is exposed to a source, the incident photon energy is absorbed by the material. Then electrons move from a ground state to an excited state. When they return to the ground state, they release the excess energy in the form of photons as shown in figure 2.3. The resulting wavelength is higher than the wavelength of the photon source.
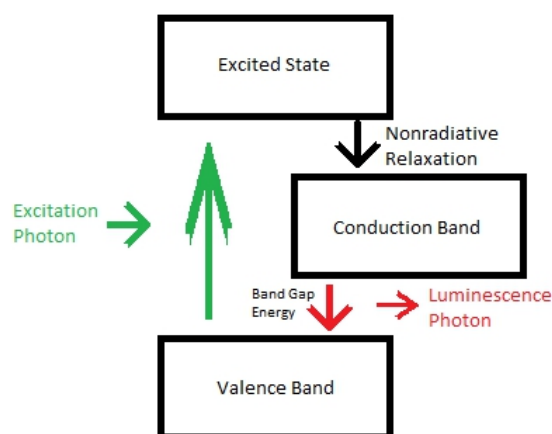
Figure 2.3: Basic Principle of Luminescence

In the past decade, some researchers have prepared nanocomposites that present luminescence by incorporating inorganic compounds, which are interesting due to their optical properties, in an organic matrix acquiring properties of both the nanoparticles and the matrix to adapt their physical and chemical properties[45–48].

Zinc oxide (ZnO) is an inorganic compound that is insoluble in water. ZnO is an excellent semiconductor which has a good transparency, thermal stability, biocompatibility, low cost, low toxicity, high mobility of electrons and strong luminescence at room temperature[49,50]. ZnO presents a direct band gap in 3.37 eV at room temperature. It produces UV emission at 370 nm due to direct exciton transition[51,52], and visible emission which has been attributed to Zn vacancies[53,54], O vacancies[54–57], Zn interstitials[58], O antisites[59] and transitions from Zn interstitials to Zn vacancies[60]. For these reasons, it is widely used in electronic devices such as light emitting diodes or thin-film transistors. The chemical, mechanical, electrical, structural, morphological, and optical properties of ZnO depend on the size, composition, morphology, and crystallinity[61–65].

2.2.1   Luminescence of Chitosan

CS has demonstrated to be a solvent, stabilizing, and reducing medium for photonic applications. However, there are few studies about the processes which involved CS photoluminescence. An emission band in the visible spectrum at 465 nm with a laser excitation of 369 nm has been reported and attributed to the amine groups of CS[66]. Furthermore, the luminescence of CS in different concentrations has been investigated under an excitation of 325 nm to get emission wavelengths from 400 to 415 nm[67,68]. This proved that the emission wavelength of CS can be affected by its concentration, which may result in redshifts. On the other hand, CS system can be either stabilized or synthesized with a luminescent agent or plasmonic NPs such as gold or silver to emit a good intensity of light[69]. The most common luminescent systems of CS use europium complex like $Eu(CF_3SO_3)_3$ to get a good luminescence properties for possible applications in electrochemical devices[70–72].

2.3   Characterization Techniques

There exist several ways to characterize thin films, here are a brief description of the characterization techniques used in the present work is given.

2.3.1   Scanning Electron Microscopy

Scanning Electron Microscopy (SEM) is a technique that uses an electron beam to interact with the sample by producing several signals like secondary electrons, backscattered electrons, and characteristic X-rays. Basically, electron beam hits the sample surface penetrating to a low depth, which depends on the accelerating voltage and the density of the sample. This interaction produces signals which are collected by one or more detectors to give information about the topography and particle distribution[73].

The signals produced depend on the atomic number of the specimen and the beam energy. With the increase of the specimen atomic number, the volume and depth of the electron penetration decrease because the number of particles in specimen increases, stopping the penetration of electrons. However, with the increase of the beam energy, the volume and depth of the penetration increase[74,75].

Secondary electrons are used to visualize the texture and roughness of the surface. These electrons give information about the topography with good resolution. Backscattered electrons are used to give information about features that are deep beneath the surface, such as composition. They also provide topographic information, however, this information differ from secondary electrons because some backscattered electrons are blocked by regions of the specimen. Characteristic X-rays give information about chemical composition of the specimen[74,75].

2.3.2   Fourier Transform Infrared Spectroscopy

Fourier Transform Infrared Spectroscopy (FTIR) is a technique which uses electromagnetic waves to interact with the sample in the infrared region, where these waves couple very well with the molecular vibrations. Thus, when interaction occurs at a certain frequency, an excitation is caused in molecules that reach a higher vibrational state that

helps them absorb infrared radiation, providing information on the chemical composition (the functional groups) of the sample. The axes of the FTIR spectrum are given by the corresponding wavenumber against values of transmittance or absorbance values[76–78].

Electromagnetic radiation is a combination of an electric field and a magnetic field that change or oscillate periodically at the same frequency, but perpendicular to each other. These waves are propagated to a constant velocity c, which is known as the velocity of the light of electromagnetic waves. c is given by the next equation[79]:

$$c = \lambda v \tag{2.1}$$

where λ and v are the wavelength and frequency, respectively. The wavelength is the distance between two positions in the same phase. Frequency is the number of oscillations or vibrations per unit time. The number of waves per unit length is known as the wavenumber. The relation between the wavenumber and frequency is given by[79]:

$$v = c\bar{v} \tag{2.2}$$

The vibrational frequencies of any chemical group depend on both the type of atoms involved and the type of chemical bonds. These frequencies are expected in specific regions[80].

2.3.3 Powder X-Ray Diffraction

X-Ray Diffraction (XRD) is a technique used to determine the crystalline or amorphous structure of sample using a focused X-ray beam in sample, where will occur an interaction inside of sample causing that a beam of incident X-rays to diffract into many specific directions. These X-rays diffracted will be collected by a detector resulting in peak positions and intensities that are used to identify the phase of the material[81,82]. A diffractogram is the result of a XRD measurement. This diffractogram is compared with a reference pattern from an international recognized database[83].

A diffractogram shows phases which are present (peak positions), concentrations of these phases (peak heights), amorphisation content (background hump), and crystallite size (peak widths). X-rays are generated by a cathode ray tube, filtered to produce monochromatic radiation and collimated to concentrate the rays towards the sample. An interaction is caused between the incident X-rays and the sample which generates constructive interference when conditions satisfy Bragg's law. This states that when X-rays beam, that is monochromatic and coherent, hits on a crystal surface at an angle θ, scattering occurs. The scattered rays also occurs at angle θ, and depend on both the number and distribution of the electrons at the lattice sites. The Bragg's Law is expressed as[83]:

$$n\lambda = 2d\sin\theta \tag{2.3}$$

where λ, d, θ and n are the wavelength of incident X-rays, the interplanar spacing, the angle of incident X-ray and an integer, respectively. Each crystal has own characteristics such as the size and arrangement of its atoms so it has interplanar spacings that are inherent in it. These interplanar spacings determine the angles at which strong X-ray diffractions occur. They are the fingerprint of a crystalline compound and can be used to identify them. Diffraction

occurs when there are highly regular structure, as for example, crystalline solids. Therefore, amorphous materials will not diffract[83].

Unlike the crystal structure where X-rays are scattered in certain directions when they hit the formed lattice planes causing high intensity peaks, in an amorphous structure X-rays are scattered in many directions leading to a large bump distributed in a wide range (2θ) instead of high intensity narrower peaks. This means that a broad peak for amorphous structures and a sharp peak for crystalline materials.

A powder X-ray diffractometer makes the sample to rotate in the path of the collimated X-ray beam at an angle θ while the X-ray detector rotates at an angle of 2θ to collect the diffracted X-rays. Data for typical powder patterns are collected at 2θ from 5° to 70°. XRD is used to analyze materials such as polymers, thin film, semiconductor, metals, etc. With this analysis, defects can be detected in a particular crystal[84].

2.3.4 Complex Impedance

Electrochemical Impedance Spectroscopy (EIS) is a usually technique used to measure impedance, resistance capacitance or conductivity of electrochemical systems. The ability of these systems to resist the flow of electrical current is known as resistance and follows Ohm's law[85]:

$$R = \frac{V}{I} \tag{2.4}$$

where R, V and I are resistance, voltage and current, respectively. However, resistance is replaced by the impedance as a more general circuit parameter[86]. Hence, resisting the flow of electrical current is known as impedance in electrochemical systems. It can be measured by applying an oscillating voltage, and measuring the current response[87,88] as shown Equation 2.5,

$$\begin{aligned} \mathbf{Z} &= \frac{V}{I} \\ &= \frac{|V|sin(\omega t)}{|I|sin(\omega t + \theta)} \end{aligned} \tag{2.5}$$

where $\mathbf{Z}$, $|V|$, $|I|$, ω, t and θ are impedance, the amplitude of the voltage signal, the amplitude of the current signal, the angular frequency, time and the phase shift, respectively. Impedance has also a complex representation and is defined as[89]:

$$\mathbf{Z} = Z' + iZ'' \tag{2.6}$$

where Z' and Z" are the real and imaginary part of impedance, respectively. The resistance of a circuit to the flow of electrical current is known as real impedance. While the storage of electrical energy in a circuit is known as an imaginary impedance[90]. Z' versus Z" data are presented as a plot of Nyquist. This graph provides information on the resistance of the sample taken data from the intercept of the plot with the real impedance axis as shown Figure 2.4. The Nyquist graph usually contains several semicircles, although sometimes only a part of them can be seen. At higher frequencies, film resistance can be found.

When an external voltage V and a uniform current I are applied to a sample, the resistance is defined as:

$$R = \frac{\rho t}{A} \tag{2.7}$$
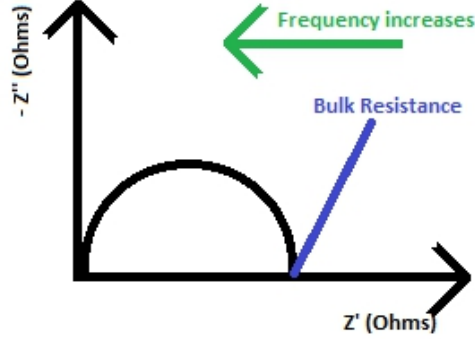
Figure 2.4: Basic Principle of Nyquist Plot

where ρ, t and A are the specific electrical resistivity of a material, thickness and area of the sample, respectively. The inverse of electrical resistivity is conductivity. Conductivity is the ability of a material to conduct electrical current between two bounding electrodes[87]. Therefore, having the value of the resistance, the conductivity can be calculated from the following equation[91,92]:

$$\sigma = \frac{t}{RA} \tag{2.8}$$

where R, t and A are the bulk resistance, thickness and area of the sample, respectively.

2.3.5 Complex Permittivity

Complex permittivity is important to know the propagation of the electric fields (behavior and interaction with the material)[93,94]. It is a complex function which depends on some parameters such as frequency or temperature[95]. It can be defined using both dielectric constant (real part) and dielectric loss (imaginary part). From the impedance data (Z' and Z"), one can calculate the real and imaginary parts of complex permittivity (ϵ^*) using the next equations[4,96,97],

$$\epsilon' = \frac{Z''}{\omega C_o(Z'^2 + Z''^2)} \tag{2.9}$$

$$\epsilon'' = \frac{Z'}{\omega C_o(Z'^2 + Z''^2)} \tag{2.10}$$

where ω is the angular frequency ($\omega=2\pi f$), C_o is the vacuum capacitance ($C_o=\epsilon_o A/t$, where ϵ_o is the permittivity of free space, A is the electrode cross sectional area and t is the film thickness), and ϵ' and ϵ'' are the dielectric constant and dielectric loss, respectively. Dielectric constant is the ability of a material to store electrical energy. This represents the alignment of dipoles. While dielectric loss represents the ionic conduction component[87]. When increasing conductivity of a material, dielectric constant also increases[98].

2.3.6   Ultraviolet-Visible-Near Infrared Spectroscopy

UV/Vis/NIR Spectroscopy is used to measure optical properties of samples by considering the absorption over an extended spectral range. Light energy hits the sample, which must match the energy difference between a possible electronic transition within the molecule. A fraction of this energy is absorbed by the molecule causing a electron excitation from ground state to an excited state. The excited state of an electron depends on the wavelength of the incoming light. A spectrometer records the sample absorption at different wavelengths.

From these values, the optical band gaps can be calculated using the Tauc relation given by the following equation[99],

$$\alpha h\nu = A(h\nu - E_g)^n \tag{2.11}$$

where α, $h\nu$, A, E_g and n are the absorption coefficient, the incident photon energy, a constant, energy band gap and n is the exponent. The n value depends on the electronic transition type (of the sample as well as its preparation). This value can be 1/2, 2, 3 or 3/2 for direct allowed transition, indirect allowed transition, direct forbidden transition and indirect forbidden transition, respectively[100].

The absorption coefficient can be calculated by Eq. 2.12[101],

$$\alpha(\lambda) = 2.303(\frac{A}{t}) \tag{2.12}$$

where A and t are the absorption in a specific wavelength and thickness of the sample, respectively.

On the other hand, the photon energy can be calculated by Eq. 2.13[102],

$$h\nu = \frac{hc}{\lambda} \tag{2.13}$$

where h, c and λ are the Planck constant, the speed of light in the vacuum and the wavelength, respectively. However, the photon energy can be expressed in electron volts, using the wavelength in nm, the equation can be rewritten as,

$$h\nu(eV) = \frac{1240}{\lambda(nm)} \tag{2.14}$$

The optical band gap values are extracted from a straight line of the $(\alpha h\nu)^{1/n}$ versus $h\nu$ plot. This line intersects the X-axis at $(\alpha h\nu)^{1/n}=0$. Thus, the energy band gap can be estimated from this intercept[103].

2.3.7   Photoluminescence Spectroscopy

Photoluminescence spectroscopy (PL) is an optical technique that performs a photon excitation process followed by the emission of photons to test the electronic structure of the materials[104]. It helps to determine the band gap, purity, crystal quality, levels of impurity defects of the semiconductor material and to understand the underlying physics of the recombination mechanism[105]. PL is the spontaneous emission of light from a material under optical excitation.

This light emission occurs by the photoexcitation of a sample where it absorbs the light that was directed towards it and dissipates the excess energy through the emission of light (or luminescence).

The PL principle consists of lighting the sample with photons of a source of excitation (usually ultraviolet light) that are sufficiently energetic to excite the electrons and activate the PL[106]. Sample absorbs energy in the form of photons and leads the electrons to an excited state. When these electrons return to the groundstate, in certain materials, the excess energy is released in the form of photons. This emission is collected on the computer using an optical fiber from the spectroscope. As a result, an intensity curve in arbitrary units (a.u.) as a function of the wavelength are displayed in a spectrum[107].

Luminescence has different mechanisms such as charge transfer, donor-acceptor and long afterglow. Charge transfer luminescence is when transition occurs from the orbital of one ion to the orbital of other ion. In this mechanism, the nature of bond and charge distribution of the optical cente can change. Donor-acceptor luminescence is when transition occurs between neutral donor and neutral acceptor. This mechanism of luminescence exhibits in semiconductor which are doped with both p-type and n-type impurities. Long afterglow luminescence is when inside the lattice, a photo-excited ion is trapped emitting visible light after sometime[108]. The luminescent substance will emit light at a specific wavelength that will not depend on the incident radiation[109]. Luminescence of a substance depends on both molecular structure and chemical environment[110].

Photoluminescence can occur in the form of fluorescence (short lifetime) and phosphorescence (long lifetime). Fluorescence occurs when excited species are relaxed to the ground state, releasing their excess energy as photons. While phosphorescence occurs very slowly to re-emit the radiation that material is absorbing[111,112].

Chapter 3

Methodology

3.1 Experimental Part

3.1.1 Materials

Chitosan flakes, from shrimp shells ($\geq$ 75% deacetylated) and white powder of zinc oxide were purchased from Sigma-Aldrich. Lithium perchlorate was received as a white crystalline salt from Sigma-Aldrich and acetic acid (glacial) 100% from Merck KGaA. Distilled water was used throughout the whole experiment, and all samples were prepared by solution cast technique.

3.1.2 Preparation of Chitosan Films

Aqueous solution of CS was prepared by dissolving 0.1 g of chitosan in 10 mL of acetic acid aqueous solution (1% v/v). The solution was stirred at room temperature until the solution is homogeneous. After the complete dissolution of chitosan, the solution was stored at plastic petri dish and left to dry at room temperature.

3.1.3 Preparation of Chitosan/Lithium Perchlorate films

The solution of chitosan (0.1 g CS in 10 mL acetic acid 1%) was prepared under magnetic stirring until the chitosan powder got completely dissolved. Lithium perchlorate salt was added in to the 10 mL chitosan solution to have 10, 25, 30 and 40% lithium perchlorate salt (with respect to weight of chitosan in the solution). After 15 min of stirring, the solution were poured into a plastic petri dish and dried at room temperature for 3 days.

3.1.4 Preparation of Chitosan/ZnO films

0.1 g CS was dissolved in 10 mL of 1% (v/v) aqueous acetic acid using magnetic stirring until the solution is homogeneous at room temperature. Subsequently, 0.001 g ZnO (1% with respect to weight of chitosan in the

solution) were dispersed in approximately 1 to 2 mL of distilled water and then were added into chitosan solution. The reaction mixture was again stirred to disssolve all ZnO. The mixture was casted in a plastic petri dish at room temperature.

3.1.5   Preparation of Chitosan/Lithium Perchlorate/ZnO films

$LiClO_4$ salt was dissolved in 10 mL chitosan solution by stirring until it was homogeneous. ZnO was dispersed in approximately 1 to 2 mL of distilled water and poured slowly into this solution. Different proportions were made to form films and observe the differences. ZnO were 1% with respect to weight of chitosan in the solution and $LiClO_4$ salt was 10, 25, 30 and 40% with respect to weight of chitosan in the solution. All mixtures were poured into a plastic petri dish and dried at room temperature for 3 days.

3.1.6   Summary of the compositions of each solution

The prepared solutions which were dissolved in 10 mL of 1% (v/v) aqueous acetic acid with their respective composition can be seen in the table 3.1 or figure 3.1.

Table 3.1: Composition of Hybrid Compound

Sample	CS [g]	$LiClO_4$ [g]	ZnO [g]
A	0.1	0	0
B	0.1	0.01	0
C	0.1	0.025	0
D	0.1	0.03	0
E	0.1	0.04	0
F	0.1	0	0.001
G	0.1	0.01	0.001
H	0.1	0.025	0.001
I	0.1	0.03	0.001
J	0.1	0.04	0.001

3.2   Measurement of films

3.2.1   Scanning Electron Microscopy

The surface morphology of the samples was observed using a scanning electron microscopy (SEM) called INSPECT, FEI brand with the programs called xT Microscope Server and xT Microscope Control.

Films were cut with scissors, mount on a aluminum stub with the help of a double-sided carbon tape, and are covered with gold to make film more conductor on a vacuum desk before observation. Then, they were immediately
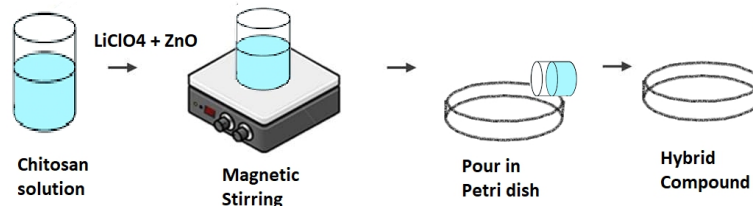
Figure 3.1: Schematic representation of the preparation of the hybrid compound

inserted into the base of the chamber. An area of interest was looked to collect it in the computer. The procedure was repeated in different areas of the sample.

3.2.2 Fourier Transform Infrared Spectroscopy

The functional groups of chitosan films with and without modifications were characterized by using Fourier Transform Infrared Spectroscopy (FTIR). The spectrophotometer used was Perkin Elmer model Spectrum 100, and by using a program called Spectre, the data of the samples were acquired in the absorbance mode at room temperature to probe the vibrational spectra of the samples.

When using FTIR program, it is essential to make a background of the air contained in the chamber to consecutively open the lid of the equipment to place the sample holder inside, and close it. Then, the program is ready to run. Finally, the lid is opened to remove the sample and exchange it for the next film.

Films were cut into circles so that they could be placed in the sample holder. Then, the FTIR spectra of films were recorded in the range from 450 to 4500 cm^{-1}.

3.2.3 X-Ray Diffraction

The diffraction patterns of the samples were obtained with X-ray diffractometer called PANalytical X'Pert pro by using X'Pert High Source Plus y X'Pert Data Viewer programs.

When using XRD program, it is fundamental to establish some operation parameters like voltage, current, 2θ angle and counting time. Then, the equipment is ready to proceed with the reading, and to obtain the X-ray spectra.

The voltage was 40 kV and the current 30 mA. The 2θ angle was scanned between 10 and 70°, and the counting time was 10.160 s at each angle step using a Cukα radiation source (λ = 1.542 Å).

3.2.4 Electrochemical Impedance Spectroscopic

An impedance analyzer of BioLogic Science Instruments was used for the Electrochemical Impedance Spectroscopic (EIS) test of the liquid samples. Using EIS, the values of the impedance, resistance and conductivity of acetic acid,

CS, CS doped with different proportions of lithium perchlorate can be found by assembling each in an electrochemical cell.

Films were cut into small discs of 1.1 cm diameter and placed between two identical circular smooth and cleaned pin stubs electrodes with carbon tape to stick film like a sandwich. The impedance of the films was measured using the SP-150 potentiostat that was connected to a computer in the frequency range from 50 Hz to 1 MHz. An electrochemistry software called EC-Lab was used to control the measurements. The ionic conductivities (σ), equivalent circuit and dielectric properties of the blends were determined from electrochemical impedance spectra (EIS).

3.2.5   Ultraviolet-Visible-Near Infrared Spectroscopy

Optical properties of the chitosan films with and without modifications were determined by using a UV/Vis/NIR Spectrometer called Lambda 1050 and a program called UV WinLab.

Films were put in the sample holder with the help of a support. Then, the UV/Vis spectra of films were recorded in the range from 200 to 800 nm.

3.2.6   Photoluminescence Spectroscopy

The photoluminescence spectra were recorded on a High-Resolution Spectrometer called HR4000CG-UV-NIR spectrometer using a program Ocean Optics SpectraSuite. This investigation was realized with an excitation wavelength of 400 nm, and integration time of 5 seconds. Set up of photoluminescence is shown in Appendix A.

Chapter 4

Results & Discussion

4.1 Scanning Electron Microscopy

The surface morphology of the chitosan and chitosan doped with different concentrations of $LiClO_4$ were investigated using SEM. The SEM image of chitosan film (figure 4.1) shows a smooth and nonporous matrix as expected into chitosan [113]. The micrographs of chitosan containing 25% $LiClO_4$ (figure 4.2) indicate that the $LiClO_4$ was dissolved into chitosan matrix. It cannot be seen the presence of $LiClO_4$ into chitosan surface, however the interactions caused between them can be observed.
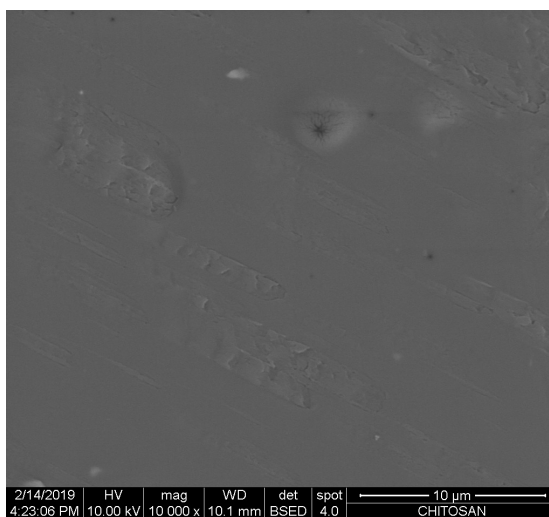
Figure 4.1: SEM image of chitosan film

Figure 4.3 shows the SEM image of chitosan containing 30% $LiClO_4$. It can be seen that the presence of 30%

(a) CS with 25% LiClO₄ with 5000 magnification.

(b) CS with 25% LiClO₄ with 10000 magnification.
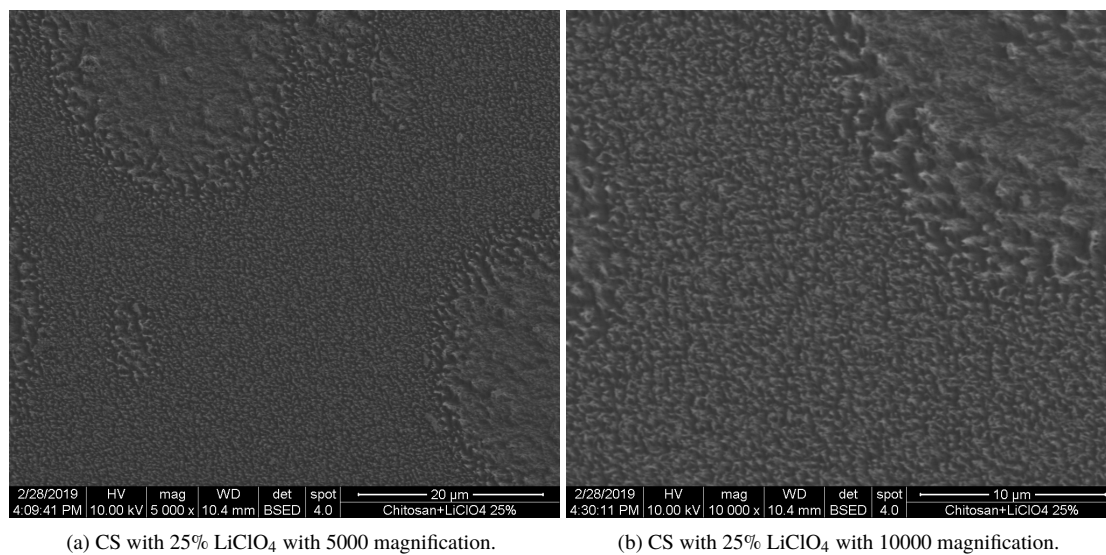
Figure 4.2: SEM images of chitosan with 25% LiClO$_4$.

LiClO$_4$ into chitosan exhibits a rough structure with some regions forming circles which could be related to the distribution of the salt in the chitosan matrix. As LiClO$_4$ concentration increases, an increase in the formation of these round features can be observed.
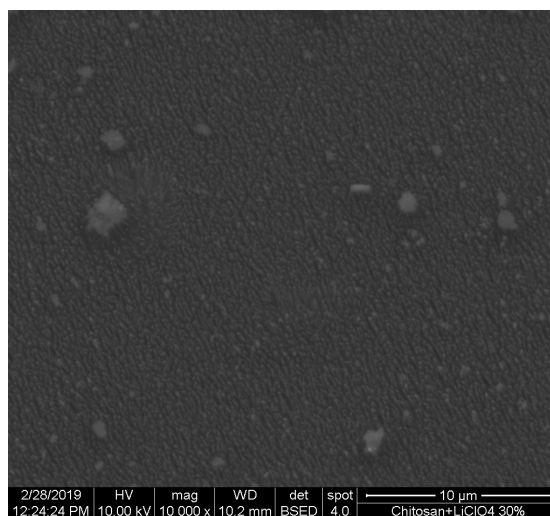
Figure 4.3: SEM image of chitosan film doped with 30% LiClO$_4$

Figure 4.4 shows the SEM image of chitosan containing ZnO and 40% LiClO$_4$. It can be seen that the hybrid

compound containing chitosan doped with ZnO and 40% LiClO$_4$ shows the ZnO dispersion, and uniformity of the chitosan surface, compared to chitosan containg 30% LiClO$_4$. ZnO seems to play an important role helping the homogeneity of the membrane, as can be observed in figure 4.4. Also, a good distribution of ZnO particles can be observed.
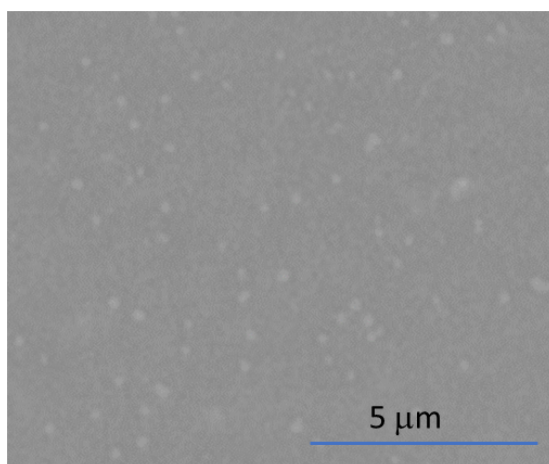
Figure 4.4: SEM image of chitosan film doped with ZnO and 40% LiClO$_4$

4.2 Fourier Transform Infrared Spectroscopy

FTIR spectroscopy was used to analyze the functional groups of the films. Figure 4.5 shows the infrared absorbance spectra of the chitosan film and chitosan doped with ZnO. The chitosan film spectrum (see figure 4.5a) shows at 3475 cm^{-1} the stretching vibration of the hydroxyl group [114,115]. The presence of broad band range of 3244 cm^{-1} is attributed to the N-H stretching [114,116,117]. The absorbance band at 2907 cm^{-1} is associated with C-H stretching [114,116–118]. The peak at 1636 cm^{-1} is assigned to the C-O stretching vibration [115,118]. The bending vibrations of N-H and C-H appear in 1549 and 1405 cm^{-1}, respectively [114–118]. The peaks at 1067 and 1144 cm^{-1} correspond to the C-O stretching mode [114–117,119]. Peak observed at 653 cm^{-1} is ascribed to the N-H twist vibration [119]. Table 4.1 demonstrates the FTIR peak assignments of chitosan. On the other hand, figure 4.5b which is chitosan with ZnO shows very similar peaks to the chitosan spectrum. Comparing these two, the vibration at 3244 cm^{-1} corresponding to the N-H stretching become broader, and the vibration at 1067 cm^{-1} shows a small change in intensity. However, figure 4.5b does not show below 560 cm^{-1} the peak corresponding to the Zn-O stretching [120–122]. It is worth noting that the absence of ZnO peaks could be related to the low amount of ZnO present or the bonding of Zn with the amide group.

FTIR studies were conducted to follow the chemical modifications in chitosan structure upon interaction with LiClO$_4$ at 10, 25, 30 and 40% (see figure 4.6). Comparing chitosan spectra with spectrum of chitosan with LiClO$_4$, there exist strong evidence which confirm the coupling of LiClO$_4$ in chitosan matrix. In general, all signals of figure 4.6b, c, d and e coincide with the principal signals of chitosan (see figure 4.6a). However, several new signals

Table 4.1: FTIR Analysis of Chitosan

Wavenumber (cm^{-1})	Types of Vibration	Functional Groups	References
3475	Stretching	O-H	[114,115]
3244	Stretching	N-H	[114,116,117]
2907	Stretching	C-H	[114,116–118]
1636	Stretching	C=O (amide I)	[115,118]
1549	Bending	N-H (amide II)	[115,118]
1405	Bending	C-H (amide II)	[115,116,118]
1144, 1067	Stretching	C-O	[114–117,119]
653	Twist	N-H	[119]
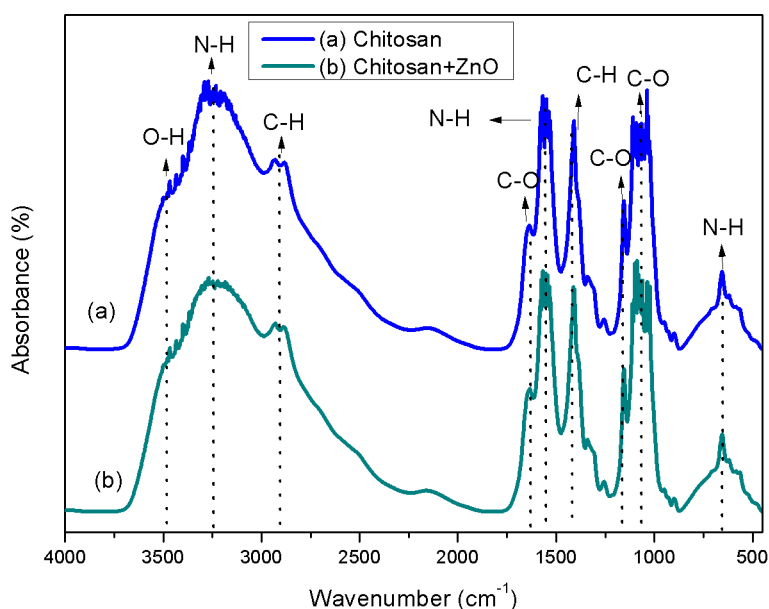
Figure 4.5: FTIR spectra of a) chitosan and b) chitosan with ZnO

appear at each one. Figure 4.6b shows a shift from 3244 to 3304 cm^{-1}, an increase in the vibration at 1405 cm^{-1}, an overlapping of the C-O peak at 1144 cm^{-1} together to the peak at 1067 cm^{-1}, and a new peak at 624 cm^{-1} corresponding to complexation and incorporation of the LiClO$_4$ can be seen. This new peak was due to ClO$_4^{-1}$ stretching, which verify then chitosan complex formation[123]. Figure 4.6c shows a shift from 3244 to 3360 cm^{-1}, a decrease in the vibration at 1405 cm^{-1}, an overlapping of the C-O peak at 1144 cm^{-1} with the peak at 1067 cm^{-1},

and the peak at 624 cm^{-1} corresponding to ClO$_4^{-1}$ stretching can be observed. Figure 4.6d shows some shifts from 3244 and 3475 to 3360 and 3554 cm^{-1} are observed, respectively. Also, an increase in the vibration at 1405 cm^{-1} is observed, and it does not show the C-O peak at 1144 cm^{-1}. The ClO$_4^{-1}$ stretching can be observed at 624 cm^{-1}. Figure 4.6 e shows some shifts from 3244 and 3475 to 3360 and 3582 cm^{-1}, respectively. It also shows an increase in the vibration at 1636 cm^{-1}, and it does not show the C-O peak at 1144 cm^{-1}. The vibration corresponding to ClO$_4^{-1}$ stretching at 624 cm^{-1} can be observed. It can be seen that figure 4.6b, c, d and e show some decreasing in the C-H bending vibration at 653 cm^{-1} due to C-Cl bonding. Furthermore, it can be observed that with the increase of the amount of LiClO$_4$, the ClO$_4^{-1}$ vibration also increases. In addition, as the LiClO$_4$ concentration increases, the interaction of the CS with the ions increases because of an unfolding is observed in the O-H and N-H bands[124].
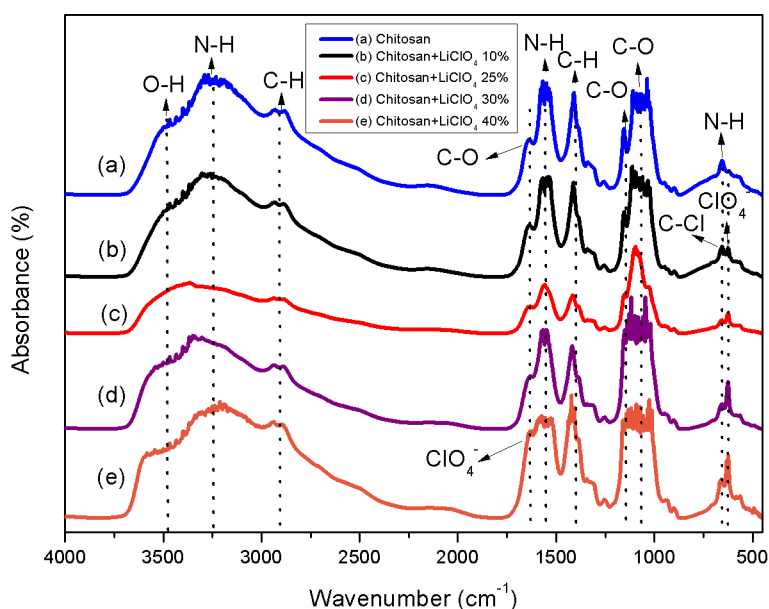
Figure 4.6: FTIR spectra of a) chitosan, and chitosan with LiClO$_4$ at b) 10%, c) 25%, d) 30% and e) 40%.

The spectra of chitosan with ZnO and the hybrid compound with different concentrations were shown in figure 4.7. Comparing this spectra with the previous spectrum (figure 4.5 and 4.6), figure 4.7b, c, d and e show the coincidence of the main peaks of chitosan doped with LiClO$_4$ and the effect caused by ZnO to reveal the formation of hybrid compound. Figure 4.7b shows an increase in intensity at 1636 cm^{-1}, the overlapping of the C-O peak at 1144 cm^{-1} together to the peak at 1067 cm^{-1}, and the peak at 624 cm^{-1} which corresponds to the incorporation of the LiClO$_4$. Figure 4.7c shows a shift in the O-H vibration from 3475 to 3546 cm^{-1}. Also, some new peaks appear at 3362, 3145 and 3089 cm^{-1} corresponding to the N-H stretching. The C-O peak at 1144 cm^{-1} disappears. Some increase in intensity appear at 1636 and 624 cm^{-1} corresponding to the ClO$_4^{-1}$ stretching. All of these confirm the

strong interaction of the hybrid compound. Figure 4.7d shows a shift in the O-H vibration from 3475 to 3571 cm^{-1}. Also, a new peak appears at 3327 cm^{-1} corresponding to the N-H stretching. The C-O peak at 1144 cm^{-1} disappears. Some increase in intensity appear at 3244, 1636 and 624 cm^{-1}. The first one corresponds to the strong interaction of the hybrid compound and the others corresponding to the ClO_4^{-1} stretching. Figure 4.7e shows a shift in the O-H vibration from 3475 to 3588 cm^{-1}. Also, a new peak appears at 3182 cm^{-1} corresponding to the N-H stretching. The C-O peak at 1144 cm^{-1} disappears. Some increase in intensity appear at 1636 and 624 cm^{-1} corresponding to the ClO_4^{-1} stretching. All these observations confirms the interaction of ZnO with lithium salt and chitosan matrix. Table 4.2 demonstrates the FTIR analysis of the hybrid compound.

Figure 4.7: FTIR spectra of a) chitosan with ZnO, and chitosan doped with ZnO and $LiClO_4$ at b) 10%, c) 25%, d) 30% and e) 40%.

4.3   X-Ray Diffraction

The phases of the chitosan films with and w/o modifications were studied by X-ray diffraction analysis. Figure 4.8 shows the XRD pattern of the films of chitosan and chitosan with $LiClO_4$. This diffractogram revealed marked differences in their structures when adding $LiClO_4$. Figure 4.8a presents peaks at 2θ = 11.94 and 18.70°. These two are characteristic peaks of chitosan which corresponding to intramolecular and intermolecular hydrogen bonds. While figure 4.8b, c, d and e do not show characteristic diffraction peaks due to the $LiClO_4$, which implies the

Table 4.2: FTIR Analysis of Hybrid Compound

Wavenumber (cm^{-1})	Types of Vibration	Functional Groups	References
3475-3588	Stretching	O-H	[114,115]
3089-3362	Stretching	N-H	[114,116,117]
2907	Stretching	C-H	[114,116,117]
1549	Bending	N-H (amide II)	[115]
1405	Bending	C-H (amide II)	[115,116]
1144-1036	Stretching	C-O	[114–117,119]
653	Twist	N-H	[119]
1636, 614	Stretching	ClO_4^{-1}	[123]

complete dissolution of salt in chitosan matrix. However, chitosan peaks show two broad peaks shifted, which promotes changes of the chitosan structure as expected for lithium salt doping. The peak at $2\theta = 11.94°$ of chitosan decreases in intensity and is located at $2\theta = 11.53°$ for chitosan containing LiClO$_4$. The main peak ($2\theta = 18.70°$) at 40% LiClO$_4$ was broader suggesting the increase in amorphization of the material with the addition of LiClO4 [125]. The formation of the chitosan complexes has been attributed to the interaction between the primary amino group with the LiClO$_4$ leading to increase in the amorphous phase [126].
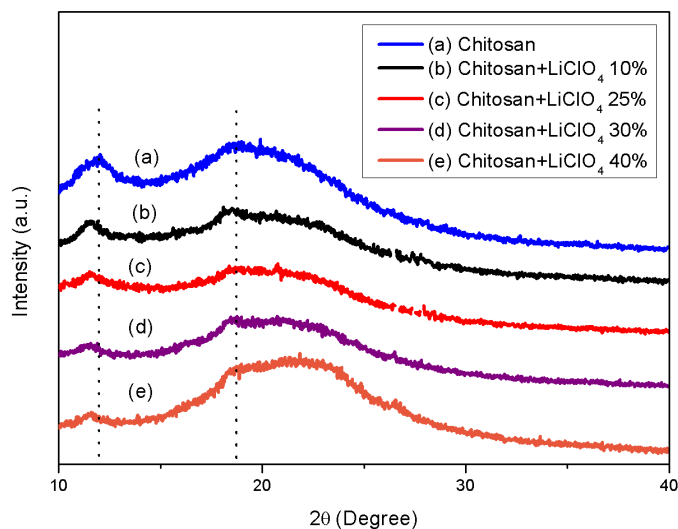
Figure 4.8: XRD pattern of a) chitosan, and chitosan doped with LiClO$_4$ at b) 10%, c) 25%, d) 30% and e) 40%.

Figure 4.9 shows the XRD pattern of the films of chitosan with ZnO and the hybrid compound. Figure 4.9a

showed peaks at 2θ = 11.87, 18.77, 42.93, and 50.22°. The first two peaks are the same chitosan peaks but there exist some differences in intensities and peak positions. The peaks of bare chitosan at 2θ = 11.94 and 18.70° become stronger and weaker and appeared at 11.87 and 18.77°, respectively [127]. The variation of them is due to incorporation of ZnO and also due to the lattice strain developed in the chitosan matrix because of the presence of ZnO [128]. Therefore, this variation confirms the presence of ZnO on the chitosan matrix. The incorporation of ZnO in chitosan increases the crystallization of the polymer and decreases its flexibility. While figure 4.9b, c, and d show the characteristic diffraction peaks of chitosan almost defined and with higher intensities at 2θ = 11.87 and 18.77° comparing to the diffractograms from figure 4.8b, c, and d, respectively. In addition, all diffractograms show the characteristic peaks of zinc at 2θ = 42.93 and 50.22°. The diffractogram from figure 4.9c shows more intensity and wider band at 18.77° suggesting a greater amorphous phase than others. However, the diffractogram from figure 4.9e does not show the peak at 2θ = 11.87, and it shows a very defined peak at 20.22° suggesting a greater crystalline phase than others.
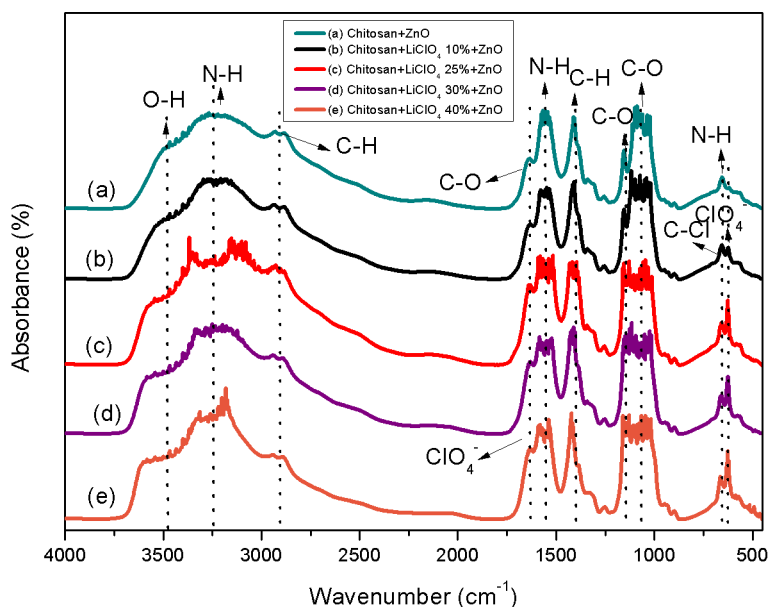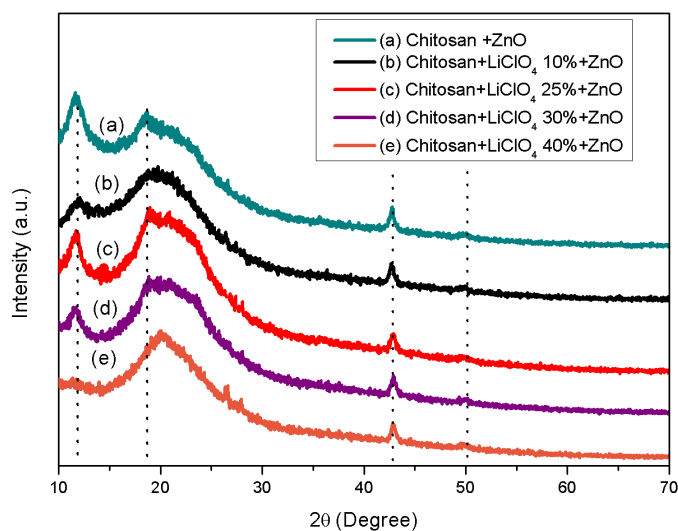

Figure 4.9: XRD pattern of a) chitosan with ZnO, and chitosan doped with ZnO and LiClO$_4$ at b) 10%, c) 25%, d) 30% and e) 40%.

4.4 Electrochemical Impedance Spectroscopy

4.4.1 Conductivity Studies

Electrochemical impedance is a powerful tool to study the ionic properties of the material. The Nyquist plots of the chitosan and chitosan with ZnO, chitosan with $LiClO_4$, and chitosan doped with ZnO and $LiClO_4$ are given in figures 4.10, 4.11, and 4.12, respectively. The Nyquist plots show the resistance of the material to the electrical current. The Nyquist plot in figure 4.10 for chitosan shows a semicircle in the higher frequency region followed by other broadened semicircle in the lower frequency region. While, similar behavior with two semicircles can be seen for chitosan with ZnO. At higher frequencies, the semicircle is ascribed by the resistivity properties of both chitosan and chitosan with ZnO, and at low frequencies, could be related with the electrodes. The diameter of the semicircle for chitosan was smaller than chitosan with ZnO. This means that addition of ZnO increases the bulk resistance.
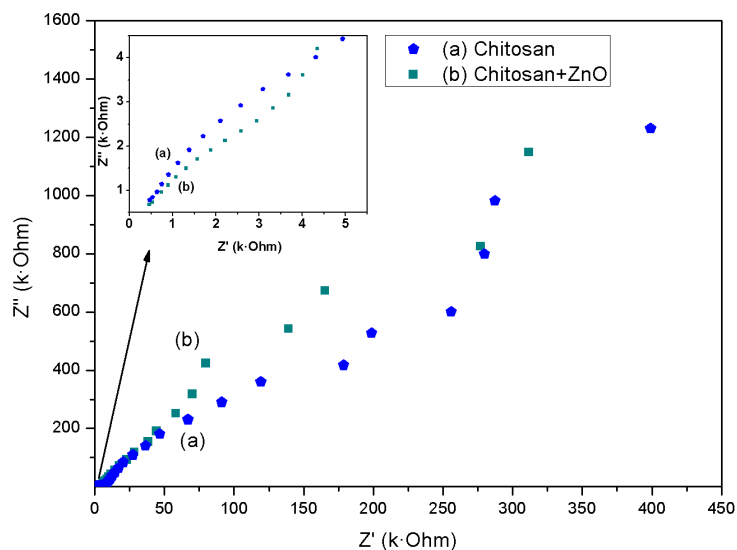
Figure 4.10: Nyquist plot for chitosan and chitosan with ZnO.

On the other hand, in order to study the increase in $LiClO_4$ concentration, the size of the semicircle of the Nyquist plots is analyzed, which displays a noticeable decrease in the resistance when increasing $LiClO_4$ concentration. Figure 4.11 shows the dependence of amount of salts of impedance spectra of chitosan with $LiClO_4$ at different concentrations as a representative plot. It can be seen that with increasing $LiClO_4$ concentration, the bulk resistance is decreasing, i.e., the diameter of the semicircle of high frequency region decreases with increase in lithium salts. As it is known, the ionic conductivity of polymer depends on the resistance, the number of charge carriers and the ion mobility[129]. This means that when adding $LiClO_4$ in CS polymer matrix, the mobility of the ions and the number of charge carriers increase, and the resistance decreases. Correlating these measurements with the XRD results, it

can be observed that the bulk resistance decreases when chitosan is more amorphous (reducing the diameter of the semicircle). It has been attributed to the decrease of the resistance to the increase of the conductivity[91,130].
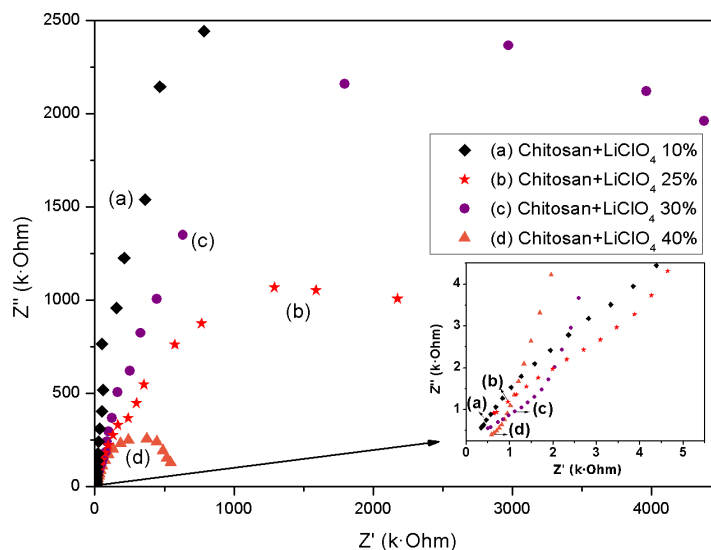
Figure 4.11: Nyquist plot for chitosan doped with $LiClO_4$.

The Nyquist plots are analyzed to display the bulk resistance (see figure 4.12). These plots show the changes caused for ZnO and different concentrations of $LiClO_4$ in chitosan matrix as a representative plot. It can be seen that chitosan with $LiClO_4$ at 25% and ZnO shows the lower semicircle compared to others. From XRD results, chitosan with $LiClO_4$ at 25% and ZnO shows the higher amorphous peak for the hybrid compound. It can be observed that amorphisation of the structure can cause a reduction in the bulk resistance of the material.

It has been reported that the amorphous phase improves the ionic transportation through polymer which aids to acquire high ionic conductivity[131]. Therefore, the ionic conductivity values of all measured samples were calculated by using the Nyquist diagram plots and Eq. 2.8[132]. The values of thickness, area, bulk resistance and conductivity of the samples are displayed in Table 4.3. The bulk resistances are taken from the intercept of the semicircle with the real axis at low frequency. The analysis of Table 4.3 reveals that the addition of $LiClO_4$ promotes an increase of ionic conductivity. The chitosan doped with ZnO and $LiClO_4$ at 10 and 40% have the same ionic conductivity values. In general, adding ZnO decreases the ionic conductivity comparing with films without ZnO. Conductivity of the chitosan film has been reported to $8.3x10^{-5}$ S cm^{-1}[133]. While, Wu *et al.* reported the ionic condutivity of chitosan to be 10^{-9} S cm^{-1}[134]. In the present work, these values differs from the value obtained $3.2x10^{-7}$ S cm^{-1}. On the other hand, Rathod *et al.* have achieved a value of $3x10^{-6}$ S cm^{-1} for a composite of chitosan, PVA and 20% $LiClO_4$[100]. Although they use a more amorphous matrix, it could be established that conductivity obtained is within the range. The highest ionic conductivity was $2.1x10^{-6}$ S cm^{-1} obtained on chitosan containing $LiClO_4$ at 40%.
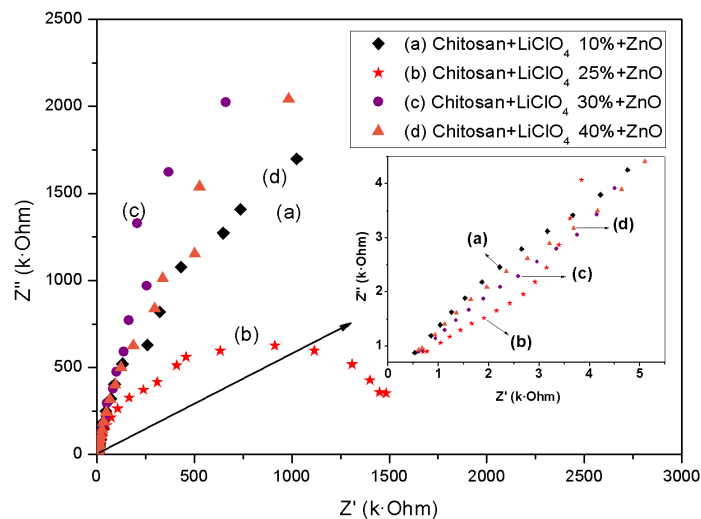
Figure 4.12: Nyquist plot for chitosan doped with ZnO and LiClO$_4$.

Table 4.3: Conductivity values for all the samples

Sample	Thickness (cm)	Area (cm^2)	Bulk resistance (Ω)	σ (S cm^{-1})
CS	4.3×10^{-3}	0.95	1.5×10^4	3.2×10^{-7}
CS+10% LiClO$_4$	4.4×10^{-3}	0.95	1.4×10^4	3.3×10^{-7}
CS+25% LiClO$_4$	4.4×10^{-3}	0.95	1.2×10^4	3.9×10^{-7}
CS+30% LiClO$_4$	4.1×10^{-3}	0.95	6.9×10^3	6.3×10^{-7}
CS+40% LiClO$_4$	4.3×10^{-3}	0.95	2.2×10^3	2.1×10^{-6}
CS+ZnO	2.1×10^{-3}	0.95	1.0×10^4	2.2×10^{-7}
CS+ZnO+10% LiClO$_4$	4.5×10^{-3}	0.95	1.6×10^4	3.0×10^{-7}
CS+ZnO+25% LiClO$_4$	3.5×10^{-3}	0.95	9.6×10^3	3.8×10^{-7}
CS+ZnO+30% LiClO$_4$	3.3×10^{-3}	0.95	1.3×10^4	2.7×10^{-7}
CS+ZnO+40% LiClO$_4$	4.3×10^{-3}	0.95	1.5×10^4	3.0×10^{-7}

To know the frequency responses of the films with phase change, the Bode plots are used. The Bode plots of the chitosan and chitosan with ZnO, chitosan with LiClO$_4$ (10, 25, 30 and 40%), and chitosan doped with ZnO and LiClO$_4$ (10, 25, 30 and 40%) are given in figures 4.13, 4.14, and 4.15, respectively. As can be seen in figure 4.13, the Bode plot of chitosan shows two phase shifts of $\phi = 76$ at high frequency ranges, and $\phi = 57$ at low frequency ranges. These phase angles at higher and lower frequency could be related to the capacitive and diffusive characteristics of

the chitosan. However, when ZnO is incorporated to the chitosan shows phase angles very similar comparing to the Bode plot of chitosan. The Bode plot of chitosan with ZnO shows two phase shifts of $\phi = 76$ at high frequencies, and $\phi = 53$ at low frequencies. These phase angles could be related to the capacitive and diffusive behavior of chitosan, or its own resistivity[135].
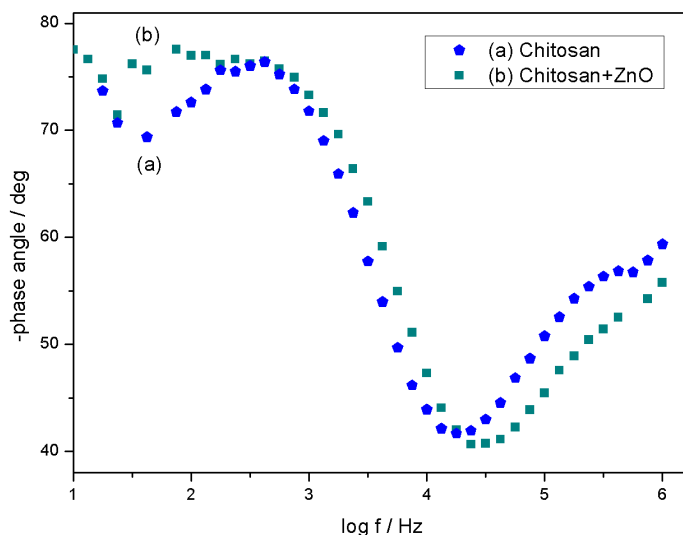
Figure 4.13: Bode diagram of chitosan and chitosan with ZnO.

As can be seen in figure 4.14, the diagram of chitosan with LiClO$_4$ at 10% shows one phase shift of $\phi = 83$ at high frequency ranges and another phase shift of $\phi = 58$ at low frequency ranges. The diagram of chitosan with LiClO$_4$ at 25% shows two phase angles of $\phi = 73$ and 55 at high and low frequency ranges, respectively. The diagram for chitosan with LiClO$_4$ at 30%, with phase angles $\phi = 71$ and 72 at high and medium frequencies, respectively. The diagram of chitosan with LiClO$_4$ at 40% shows two phase angles $\phi = 68$ and 65 at medium and higher frequencies, respectively. Comparing all of these, chitosan with LiClO$_4$ at 10% shows the maximum phase angles of $\phi = 83$ at high frequency ranges and $\phi = 58$ at low frequency ranges. These phase angles presents the minimum capacitive behavior and the maximum resistivity behavior, respectively[136]. As the LiClO$_4$ concentration increases, a more capacitive behavior can be observed[137]. Regarding to the literature, chitosan with LiClO$_4$ at 40% shows a very low resistance behavior and a high capacitive behavior[135]. Therefore, by increasing the concentration of LiClO$_4$, the phases shift to the medium frequencies which could be related to the increase of the ionic species.

As can be seen in figure 4.15, the diagram of chitosan with LiClO$_4$ at 10% and ZnO shows two phase angles of $\phi = 79$ and 56 at high and low frequency ranges, respectively. The diagram of chitosan with LiClO$_4$ at 25% and ZnO shows two phase angles $\phi = 75$ and 51 at medium and low frequency ranges. The diagram for chitosan with LiClO$_4$ at 30% and ZnO, with phase angles $\phi = 82$ and 78 at high frequencies, and 55 at low frequencies. The
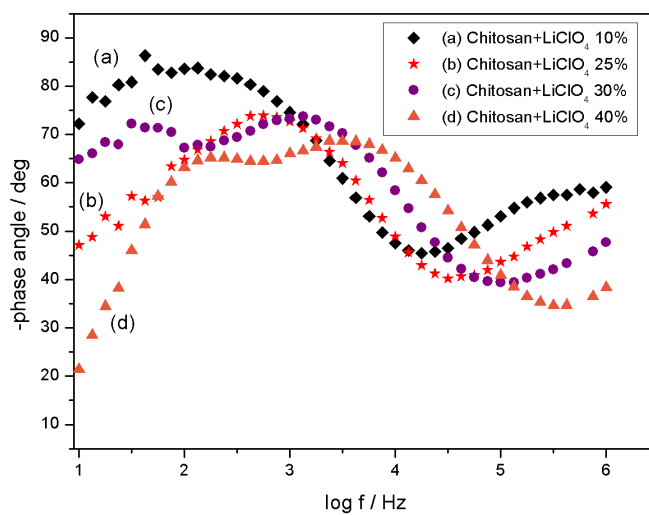
Figure 4.14: Bode diagram of chitosan doped with LiClO$_4$.
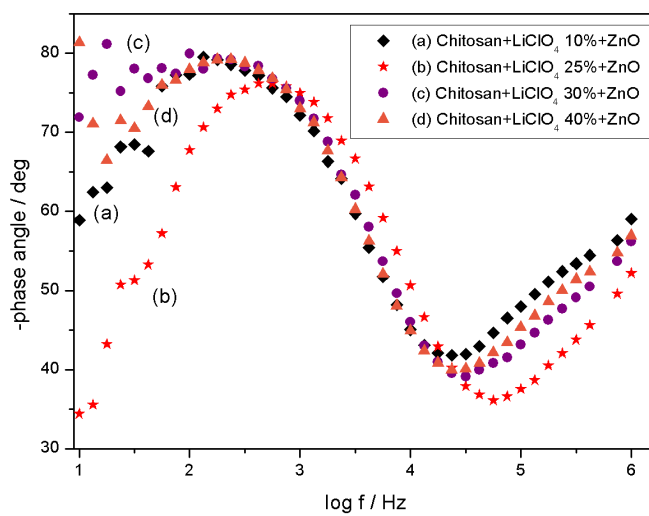
Figure 4.15: Bode diagram of chitosan doped with ZnO and LiClO$_4$.

diagram of chitosan with LiClO$_4$ at 40% and ZnO shows phase angles ϕ = 82 and 79 at high frequencies, and 56 at low frequencies. The phase angles are lower in chitosan with LiClO$_4$ at 25% and ZnO compared to others. This has been attributed to the low resistance in the material [135]. For hybrid compounds containing a LiClO$_4$ concentration greater than 25% could have free Li ions that could get too close and recombine to form Li salts that are immobile and that increases the resistance.

4.4.2   Dielectric Properties

The dielectric properties help to understand the conductivity behavior of the polymer electrolyte, since that trend can be followed. This trend is related to ion transport in polymer electrolyte [138]. The understanding of the mechanism of ion conduction together with the relaxation processes in the polymer electrolyte makes it possible to get the information of the ionic interaction in the polymer electrolyte [139]. At low frequency, it has been reported that peaks in both dielectric constant and dielectric loss can be attributed to the electrode polarization and space charge effects [140,141]. On the other hand, at high frequencies, it has been attributed to the non-excess ions for the rapid inversion of the electric field and the absence of polarization [140–143].

Figures 4.16, 4.17 and 4.18 show the dielectric constant vs. frequency for all samples at room temperature. As can be seen in these figures, the dielectric constant decreases with the increase in frequency. This has been related to the orientation of the charge carriers to the applied electric field at low frequencies [144]. The dielectric constant has been attributed for storage of charges [4].
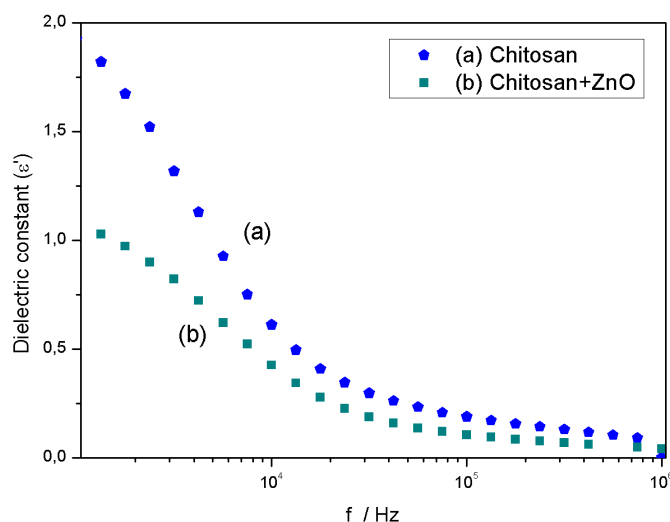
Figure 4.16: Variation of dielectric constant with frequency of chitosan, and chitosan with ZnO.

Figure 4.16 shows a greater polarization of the electrode in the chitosan than the chitosan doped with ZnO.

When chitosan is doped with ZnO, space polarization decreases in the interface of matrix leading to decrease of dielectric values. While Figure 4.17 shows that the dielectric constant is increased as $LiClO_4$ increases in the low frequency part, except for the sample with 25% $LiClO_4$. It can be seen the chitosan with 40% $LiClO_4$ shows the highest dielectric constant. This means that it has the best storage of charges. In general, with the addition of $LiClO_4$, the charge carriers are dependent of frequency up to medium frequencies. This means the charge carriers orient themselves in the field direction up to medium frequencies. This could be related to the contribution of ionic properties in films.

Figure 4.17: Variation of dielectric constant with frequency of chitosan doped with $LiClO_4$ in different concentrations.

As can be seen in figure 4.18, chitosan doped with ZnO and 25% $LiClO_4$ shows a different behavior than others. At frequency 10^4 is greater than others. This could be related to ionic interactions between them. In addition, free ions may be nearby but avoiding recombination to form Li salt. In the other cases, there are few ions in the matrix or an excess of ions that causes the formation of Li salt, avoiding the storage of charges to increase. In general, the dielectric constant is shifted to the low frequency with the incorporation of ZnO. However, for chitosan containing $LiClO_4$ can be observed in medium frequencies (see figure 4.17). These results suggest that the greatest amount of free ions can be observed in medium frequency.

Figures 4.19, 4.20 and 4.21 show the dielectric loss vs. frequency for all samples at room temperature. As can be seen, the dielectric loss decreases with increasing frequency at the low-frequency range. Figure 4.19 shows relaxation peaks for chitosan and chitosan with ZnO. However, it can be seen that figure 4.20 shows the shift of the relaxation peaks to higher frequencies as increasing $LiClO_4$ concentration, which prove that the increase in conductivity is due to the increase in number of ion mobility[100]. The addition of $LiClO_4$ increases the strength of

Figure 4.18: Variation of dielectric constant with frequency of chitosan doped with ZnO and LiClO$_4$ in different concentrations.

bulk relaxation. Chitosan with 10% LiClO$_4$ shows the higher dielectric loss (see figure 4.20). Figure 4.21 shows the dielectric loss peak at low frequencies. Chitosan with 25% LiClO$_4$ is shifted to high frequency comparing to others. This could be related to conductivity processes. In general, ϵ' and ϵ" increase as LiClO$_4$ concentration increases because increase in the number of free ions. Therefore, as the number of free ions is proportional to the conductivity [145], the conductivity also increases.

4.5   Conductivity Mechanism Model

As a discussion to explain the conductivity mechanism, a model is proposed based on the proposal of Begum *et al.*[146]. When the film is dried after adding LiClO$_4$ to the chitosan solution, both mobile and immobile (crystallites) species of lithium perchlorate and free lithium ions are formed (Fig. 4.22 (b)). Only the mobile species contribute to the conductivity when an electric field is applied. When ZnO is added to chitosan solution, ZnO particles are bonded to the chitosan membrane (Fig. 4.22 (c)) and therefore the conductivity is decreased due to the ZnO nanoparticles as they make the electron paths more difficult. Inclusion of ZnO to Chitosan/LiClO$_4$ solution results in the formation of complexes and the formation of lithium salt crystallites (that contribute to the immobile species) is enhanced during film formation (Fig. 4.22 (d)). The acceleration of crystal growth of lithium salts during film formation due to ZnO results in unavailability of more mobile species of lithium salt with a result in decreasing conductivity in chitosan/LiClO$_4$/ZnO hybrid compound when compared to that of chitosan/LiClO$_4$ films.
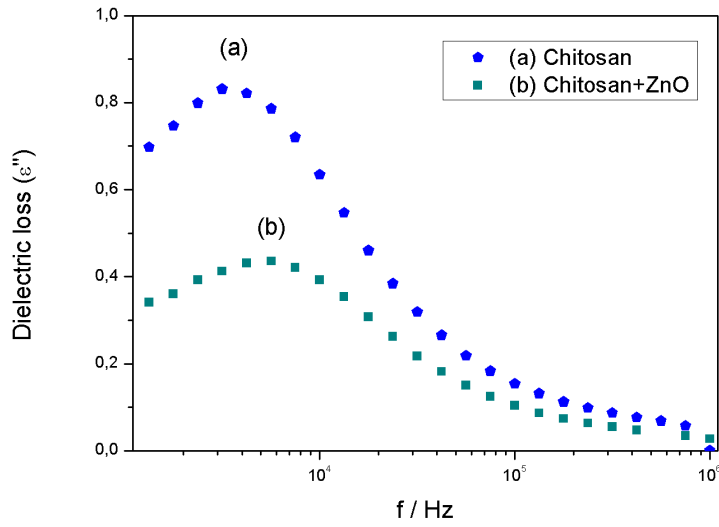
Figure 4.19: Variation of dielectric loss with frequency of chitosan, and chitosan with ZnO.
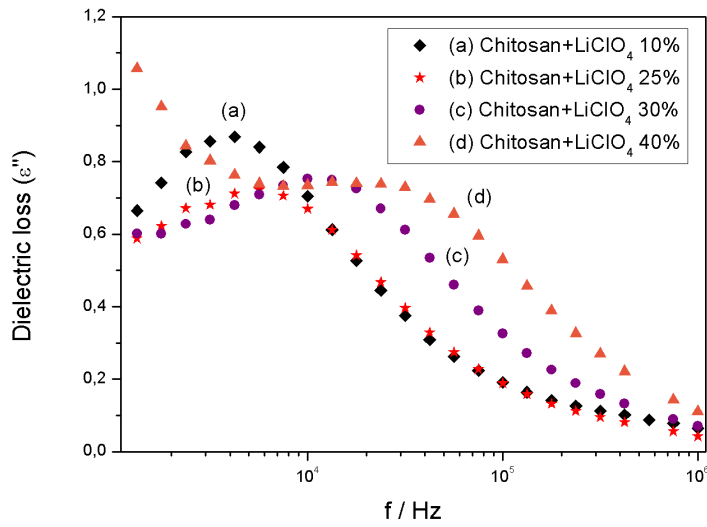
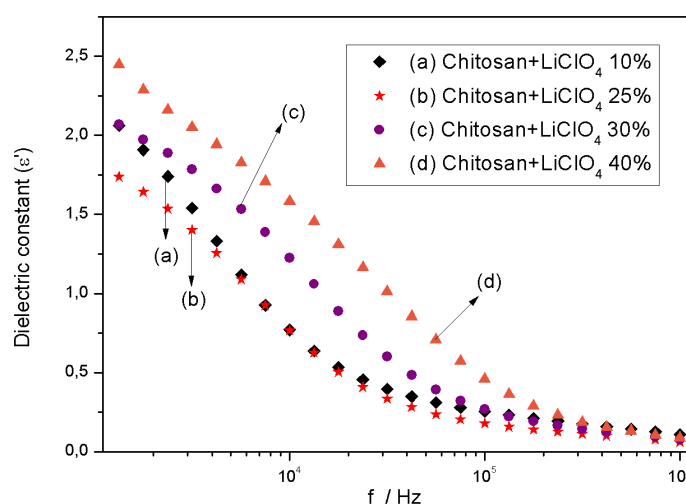
Figure 4.20: Variation of dielectric loss with frequency of chitosan doped with $LiClO_4$ in different concentrations.
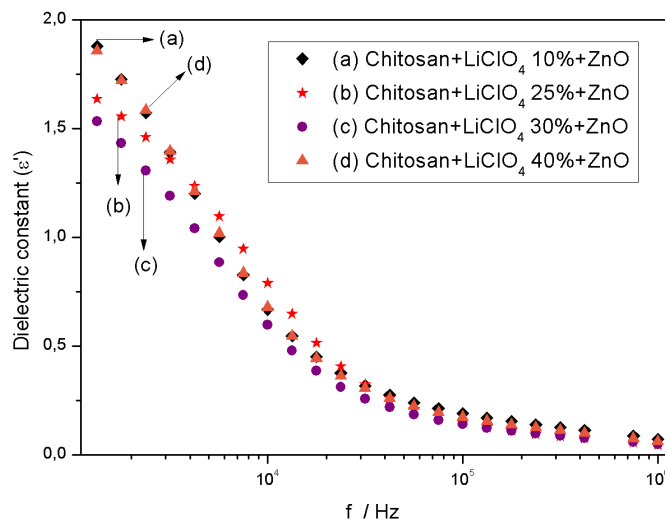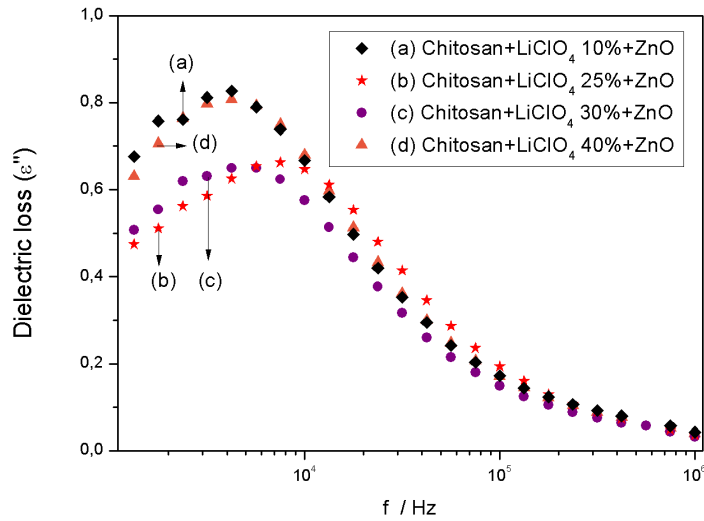
Figure 4.21: Variation of dielectric loss with frequency of chitosan doped with ZnO and LiClO$_4$ in different concentrations.
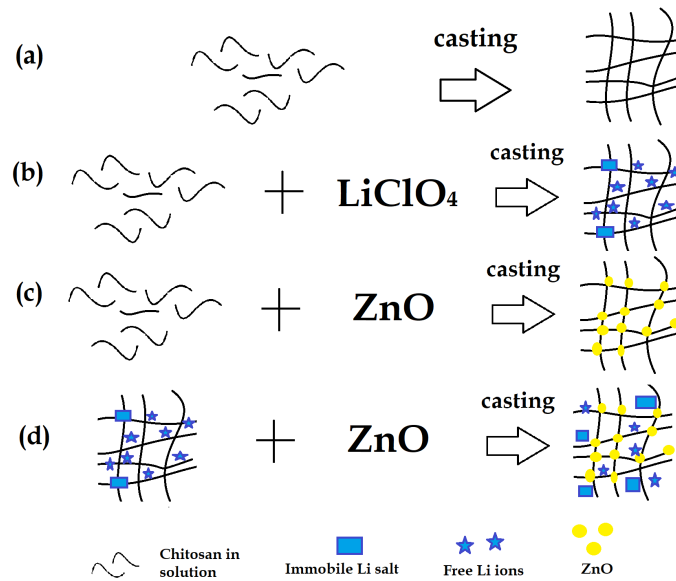
Figure 4.22: Model for formation of chitosan hybrid compound.

4.6 UV-Vis Spectroscopy

4.6.1 UV-Vis Spectrum

Figure 4.23 shows the optical absorption spectroscopy at room temperature of the chitosan (control) and chitosan containing ZnO in the UV-Vis spectral region. It can be seen from this figure that chitosan reveals two absorption peaks at 254 and 311 nm, while chitosan with ZnO shows just one wider band at 311 nm which can be attributed to the dispersion of ZnO in chitosan matrix [120,147,148]. The absorption of ZnO has occurred in the normal range and its intensity is low due to the low concentration of ZnO [149–152].
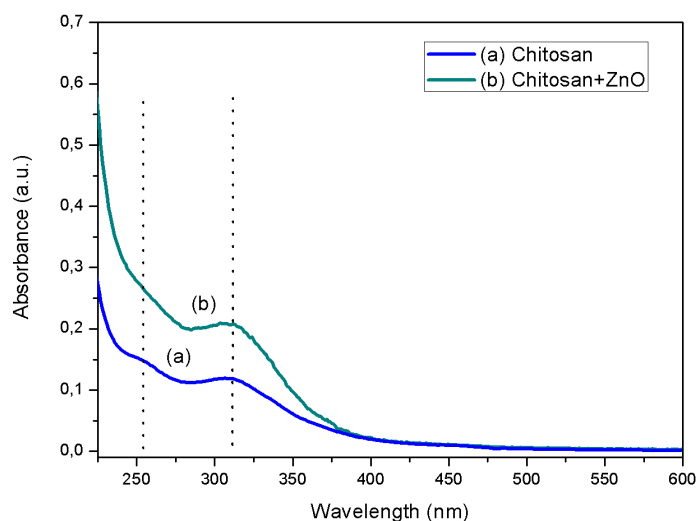
Figure 4.23: UV-Visible spectrum of a) chitosan and b) chitosan with ZnO.

The UV-visible spectrum of chitosan containing LiClO$_4$ (10, 25, 30 and 40%) are shown in figure 4.24. After incorporation of different concentrations of LiClO$_4$ in chitosan, the chitosan peaks are shifted from 254 and 311 nm to 246 and 313 nm, respectively. It can be also seen that the intensity of the absorption increases due to the increase in the salt concentration. These changes were induced due to the interaction between chitosan and LiClO$_4$. Therefore, it can be proved that the salt concentration affected the optical properties of the chitosan.

Figure 4.25 shows the absorption spectroscopy of the chitosan doped with ZnO and LiClO$_4$ at 10, 25, 30 and 40% in the ultraviolet-visible spectral region. Chitosan doped with ZnO and 10% LiClO$_4$ shows two peaks at 251 and 313 nm with low intensity. The peak is shifted from 259 to 251 nm comparing with chitosan doped with 10% LiClO$_4$. This shift could be related to the ZnO [147] and the low intensity to the low concentration of the LiClO$_4$. Chitosan doped with ZnO and 25% LiClO$_4$ shows two peaks at 251 and 313 nm. Peaks can be observed with higher absorbance. This could be related to the increase of the salt concentration. Chitosan doped with ZnO and LiClO$_4$
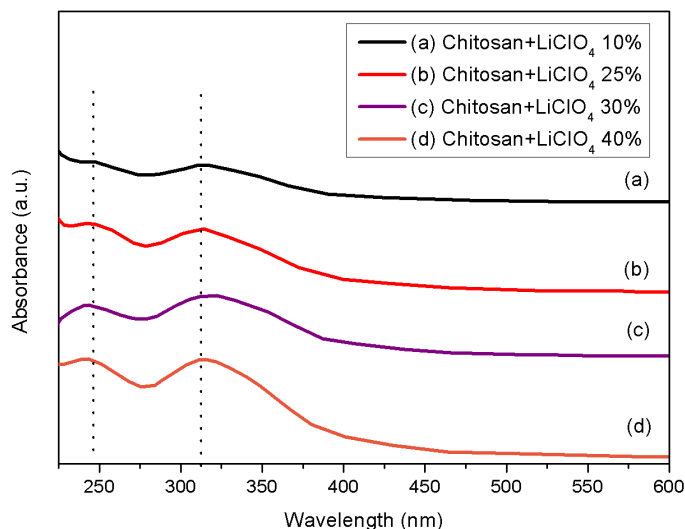
Figure 4.24: UV-Visible spectrum of chitosan doped with $LiClO_4$ at a) 10, b) 25, c) 30 and d) 40%.

at 30% and 40% show two similar peaks at 246 and 313 nm. It can be seen that the intensity of the peaks decrease with respect to chitosan doped with ZnO and 25% $LiClO_4$. This could be related to the less interaction of the salt concentration with chitosan and ZnO. Therefore, the hybrid compound ($CH/ZnO/LiClO_4$) shows its maximum absorbance when chitosan is doped with ZnO and 25% $LiClO_4$. Then, it can be proved that the salt concentration affects the optical properties.

4.6.2   Optical Band Gap

The conductivity of the polymer is related to the optical properties. From the absorption spectrum of all samples, an estimated optical band gap is calculated using Eq. 2.11 taking into account that any change observed in the optical properties affect the band gap[100]. It has been used an indirect allowed transition for chitosan systems[100,153]. Therefore, the values of the band gap are determined in a plotted graph of $(\alpha h\nu)^{1/2}$ vs. photon energy ($h\nu$) by extrapolating the straight line of the curve at the point $(\alpha h\nu)^{1/2}=0$ in photon energy-axis. The Tauc plot of the samples is shown in Appendix B and the band gap energy value for the allowed indirect transition are displayed in Table 4.4. The analysis of this table reveals that the band gap energy decreased with the $LiClO_4$ doping and further doping at 40% is the higher value. The decrease has been related to the low concentration of free electrons in the films[154]. The band gap reduction is attributed to the charge transfer of different mixtures[100].
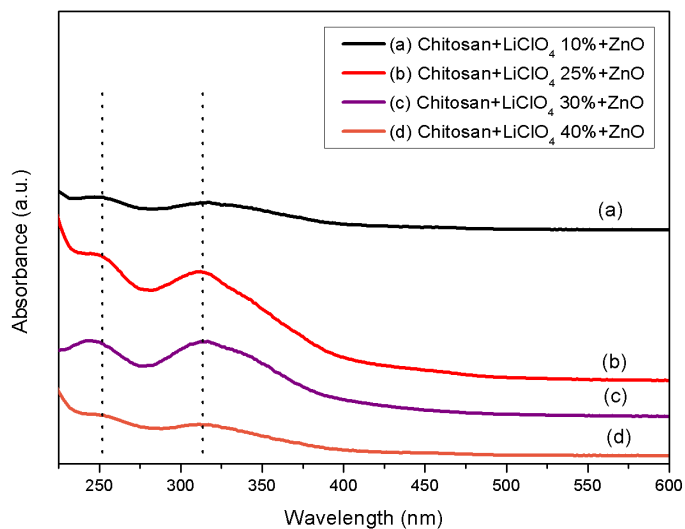
Figure 4.25: UV-Visible spectrum of chitosan doped with ZnO and LiClO$_4$ at a) 10, b) 25, c) 30 and d) 40%.

Table 4.4: The band gap values from the experimental data

Sample	Band gap (eV)
CS	2,60
CS+10% LiClO$_4$	2,72
CS+25% LiClO$_4$	2,69
CS+30% LiClO$_4$	2,77
CS+40% LiClO$_4$	2,70
CS+ZnO	2,88
CS+ZnO+10% LiClO$_4$	2,57
CS+ZnO+25% LiClO$_4$	2,57
CS+ZnO+30% LiClO$_4$	2,70
CS+ZnO+40% LiClO$_4$	2,62

4.7 Photoluminescence Spectroscopy

Photoluminescence is carried out to investigate much better the optical properties. The measurements were carried out with an excitation wavelength of 400 nm, and integration time of 5 seconds. Figure 4.26 shows the photoluminescence spectra recorded at room temperature of chitosan and chitosan with LiClO$_4$ at 10, 25, 30 and 40%. Chitosan film shows an emission peak at wavelength of 497 nm (see figure 4.26a). It has been reported that for excitation of

longer wavelength, the emission peak of chitosan could be beyond 480nm [155]. It can be seen that with increase in concentration of $LiClO_4$, the intensity of excitonic peak increases. It can be observed that chitosan doped with $LiClO_4$ at 40% shows the highest luminescence triplicating the emission value with respect to the pure chitosan. It is interesting to note that with increase in $LiClO_4$, luminiscence increases and also the ionic conductivity. Then, the influence of $LiClO_4$ on the luminescence properties of chitosan causes strong luminescence at 497 nm, which could have many important applications.
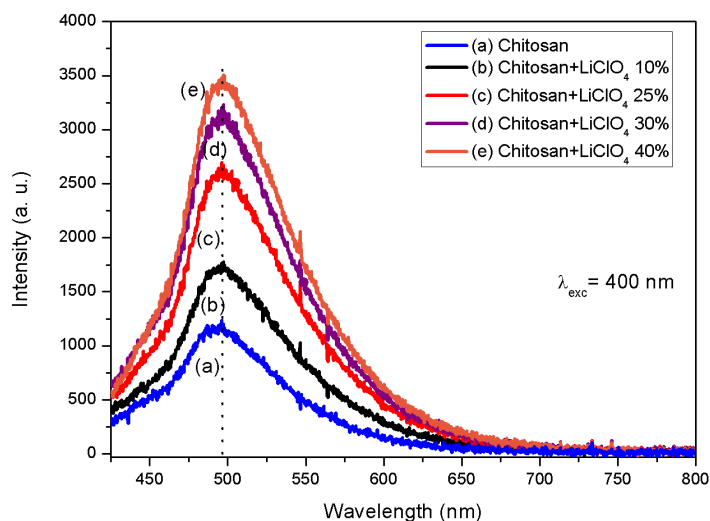
Figure 4.26: Photoluminescence spectrum of a) chitosan and chitosan doped with $LiClO_4$ at b) 10, c) 25, d) 30 and e) 40% at 400 nm excitation wavelength.

On the other hand, figure 4.27 shows the photoluminescence spectra recorded at room temperature of chitosan with ZnO and the hybrid compound at different concentrations. Chitosan with ZnO shows an emission peak at wavelength of 497 nm (see figure 4.27a). Comparing with chitosan, this peak is reduced in intensity with the addition of ZnO. For all the composite chitosan/$LiClO_4$/ZnO, the addition of ZnO decreases the luminescence intensity except for the sample of chitosan containing 25% $LiClO_4$ and ZnO. At this specific sample, luminescence and ionic conductivity are higher than others with ZnO. Correlating with XRD results, it can be seen that the peak intensity at approximately $18°$ is stronger than others. An interaction between ZnO and $LiClO_4$ at this specific concentration could be occurring to show its maximum luminescence. This means that the interaction between them modifies the structure of chitosan to show luminescence.
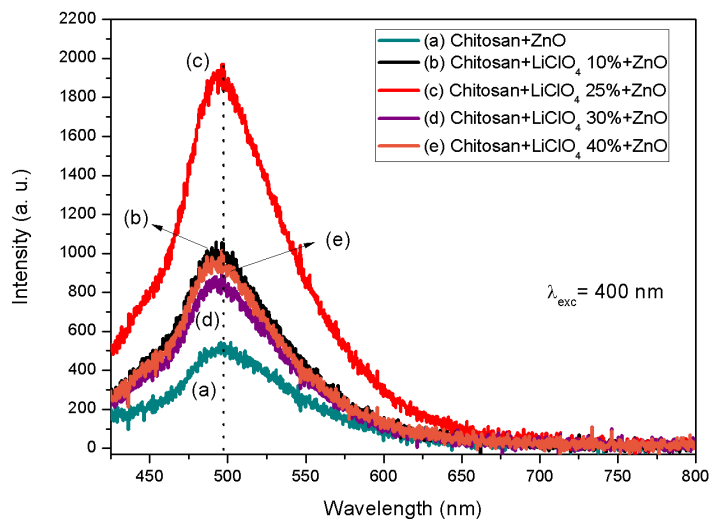
Figure 4.27: Photoluminescence spectrum of a) chitosan with ZnO, and chitosan doped with ZnO and LiClO$_4$ at b) 10, c) 25, d) 30 and e) 40% at 400 nm excitation wavelength.

4.8   Photoluminescence Mechanism Model

As a discussion to explain the photoluminescence mechanism, a model is used. When the film is excited after being illuminated (or pointed) with a laser, electrons jump from valence band to conduction band, and then when they return to valence band, they emit light. It is known that ions help electrons to move in order to occur recombination between electrons and electron holes [156]. This recombination could be reflected in the intensity of photoluminescence spectra. In few words, photoluminescence intensity could be proportional to the recombination. When photoluminescence intensity is higher, higher recombination occur between electrons and electron holes. In chitosan film occurs few recombination because it has few ions and electrons (fig. 4.28 (a)). While chitosan doped with LiClO4 (at 10, 25, 30 and 40%) have more recombination as increase their concentration (fig. 4.28 (b)). When the LiClO4 concentration increases, more mobile ions also increase. Then, these ions help electrons to move easily for recombination process, i.e. intensity increases. On the other hand, the doping of chitosan with ZnO inhibits the recombination process of charge carries (fig. 4.28 (c)). Therefore, the inclusion of ZnO in Chitosan/LiClO4 causes fewer electrons to return to the valence band, emitting less energy in the form of light (fig. 4.28 (d)).

(a) Chitosan

CB _____   CB e⁻e⁻e⁻e⁻ ___   CB e⁻e⁻e⁻e⁻ ___   CB e⁻ _____

VB e⁻e⁻e⁻e⁻e⁻e⁻   VB _____ e⁻e⁻e⁻   VB _____ e⁻e⁻e⁻   VB e⁻ e⁻e⁻e⁻e⁻e⁻

(b) Chitosan + LiClO₄

CB _____   CB e⁻e⁻e⁻e⁻e⁻e⁻ ___   CB e⁻e⁻e⁻e⁻e⁻e⁻ ___   CB _____ e⁻ _____

VB e⁻e⁻e⁻e⁻e⁻e⁻e⁻e⁻e⁻   VB _____ e⁻e⁻e⁻   VB _____ e⁻e⁻e⁻   VB e⁻e⁻e⁻ e⁻e⁻e⁻e⁻

(c) Chitosan + ZnO

CB _____   CB e⁻e⁻ _____   CB e⁻e⁻ _____   CB e⁻ _____

VB e⁻e⁻e⁻e⁻e⁻e⁻   VB e⁻e⁻ e⁻e⁻e⁻   VB ____ e⁻e⁻ e⁻e⁻e⁻   VB e⁻ e⁻e⁻e⁻e⁻e⁻

(d) Chitosan + LiClO₄ + ZnO

CB _____   CB e⁻e⁻e⁻e⁻e⁻e⁻ ___   CB e⁻e⁻e⁻e⁻e⁻e⁻ ___   CB _____ e⁻e⁻e⁻e⁻ ___

VB e⁻e⁻e⁻e⁻e⁻e⁻e⁻e⁻e⁻   VB _____ e⁻e⁻e⁻   VB _____ e⁻e⁻e⁻   VB e⁻e⁻e⁻ ____ e⁻e⁻e⁻

CB: Conduction Band   VB: Valence Band
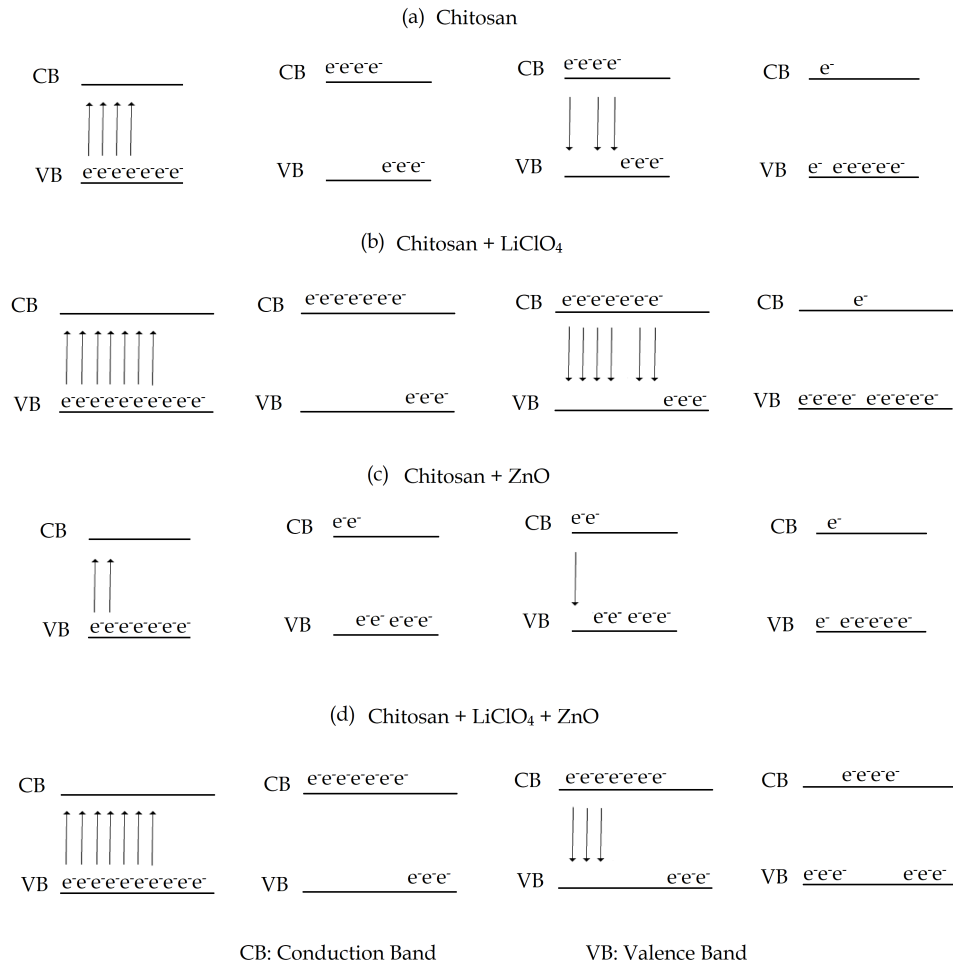
Figure 4.28: Model to explain Photoluminescence mechanism.

Chapter 5

Conclusions & Outlook

To sum up, a novel type of hybrid compound of chitosan with ZnO and $LiClO_4$ in different concentrations was synthesized. Physicochemical characterization was performed by FTIR spectroscopy and UV-Vis spectra. Strong interactions between $LiClO_4$ and chitosan were confirmed by FTIR. UV-Vis analysis revealed that the $LiClO_4$ concentration increased the absorption band. SEM results showed the salt distribution, the ZnO dispersion and uniformity of the chitosan surface. XRD results demonstrated the amorphisation of the chitosan matrix with addition of $LiClO_4$, and the crystallization induced by ZnO on CS matrix. Results of SEM and XRD suggest that $LiClO_4$ plays a vital role in composite properties. The addition of $LiClO_4$ in high concentration induces amorphization in the chitosan membrane. The resistances of the system confirmed the same results. The presence of a amorphous structure served as an evidence for the better interaction between chitosan and $LiClO_4$ which indicated that $LiClO_4$ concentration in chitosan formed polymer electrolytes. EIS technique showed the increase of the ionic conductivity as $LiClO_4$ concentrations increased. The maximum ionic conductivity at room temperature was for chitosan with 40% $LiClO_4$ with a conductivity value of $2.1\text{x}10^{-6}$ S/cm. The presence of $LiClO_4$ in chitosan resulted in higher photoluminescence of chitosan/$LiClO_4$ films. The chitosan photoluminescence was observed at 497 nm and its intensity increased by increasing the $LiClO_4$ concentration. Therefore, the hybrid compound exhibited excellent stable ionic conductivity and tunable photoluminescence, indicating their potential as a polymer electrolyte for different applications such as supercapacitors or batteries.

Appendix A

Set up of photoluminescence
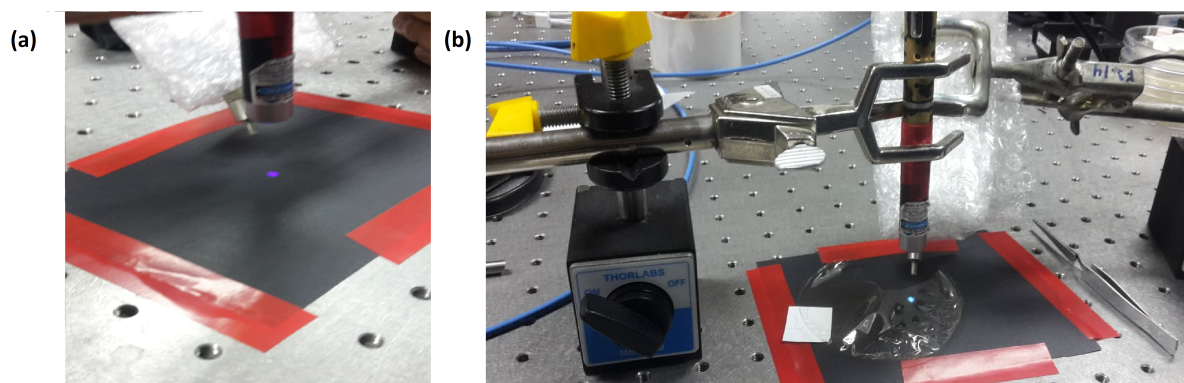
Figure A.1: Set up of photoluminescence: (a) Excitation laser of 400 nm and (b) photoluminescence of chitosan.

Appendix B

Tauc plots for band gap determination
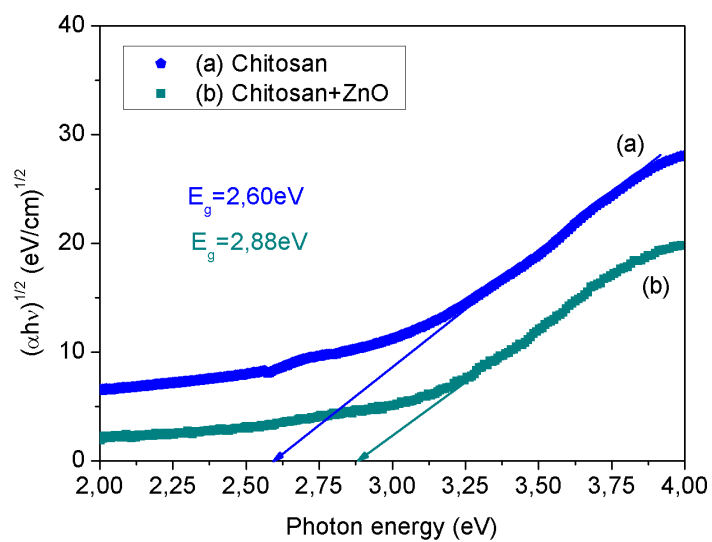
Figure B.1: Tauc plot for band gap of chitosan and chitosan with ZnO
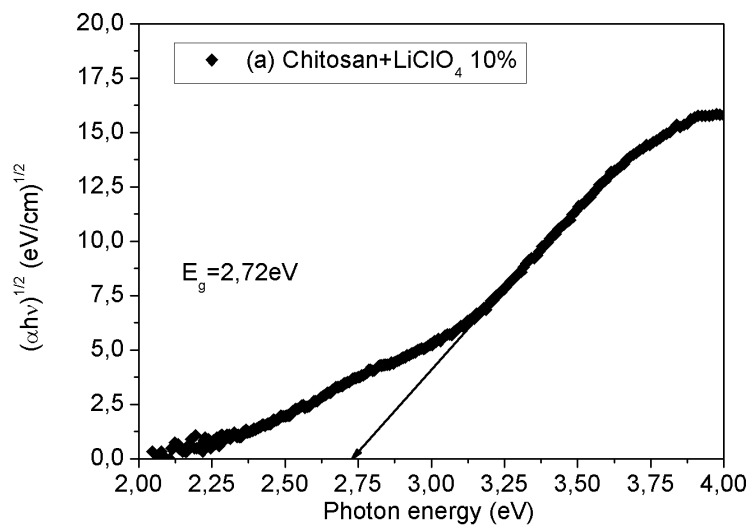
Figure B.2: Tauc plot for band gap of chitosan with 10% LiClO$_4$
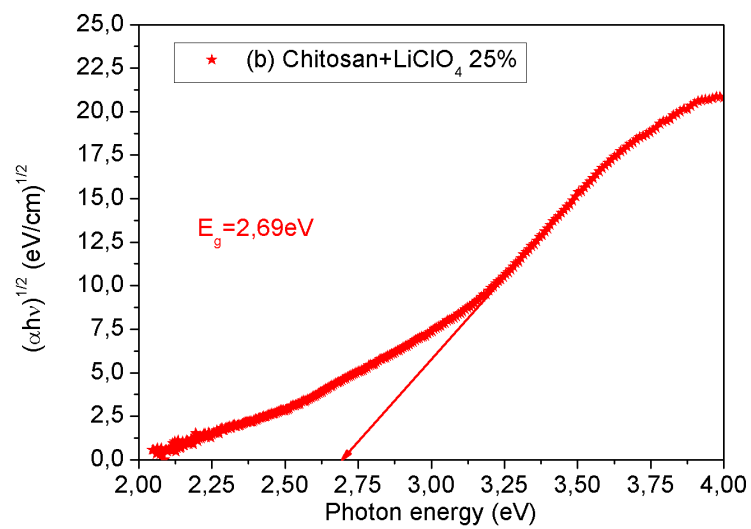
Figure B.3: Tauc plot for band gap of chitosan with 25% LiClO$_4$
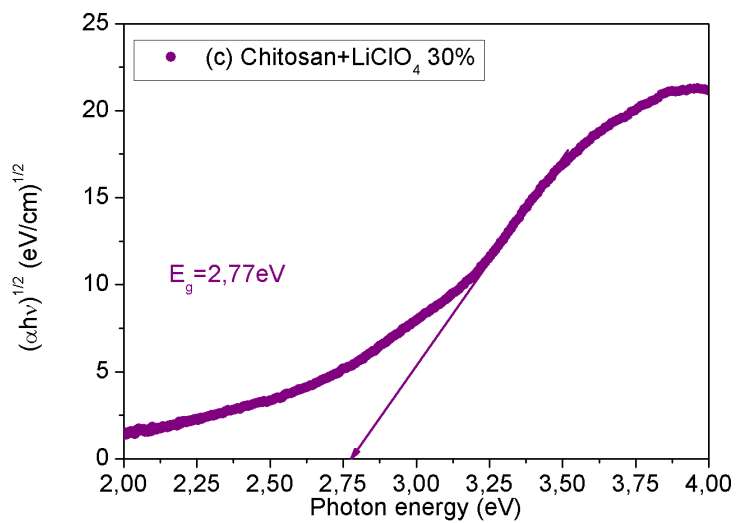
Figure B.4: Tauc plot for band gap of chitosan with 30% LiClO$_4$
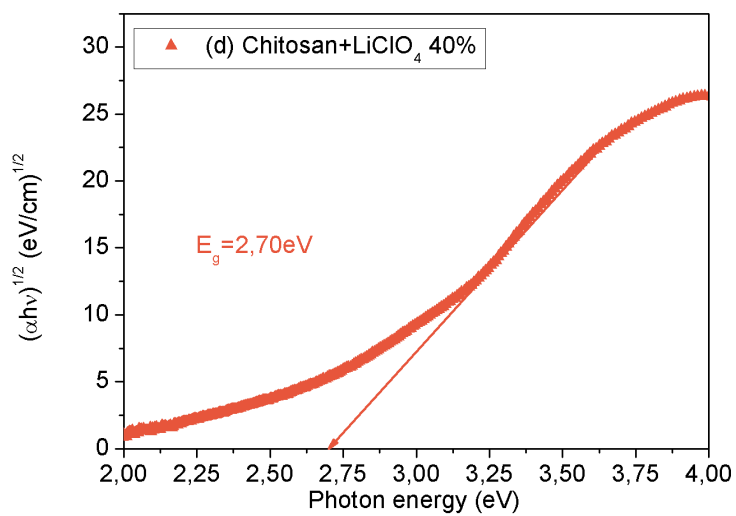
Figure B.5: Tauc plot for band gap of chitosan with 40% LiClO$_4$
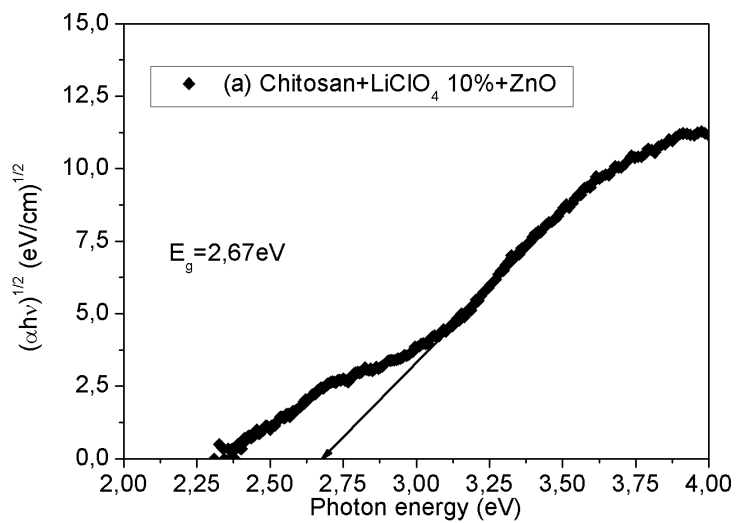
Figure B.6: Tauc plot for band gap of chitosan doped with ZnO and 10% LiClO$_4$
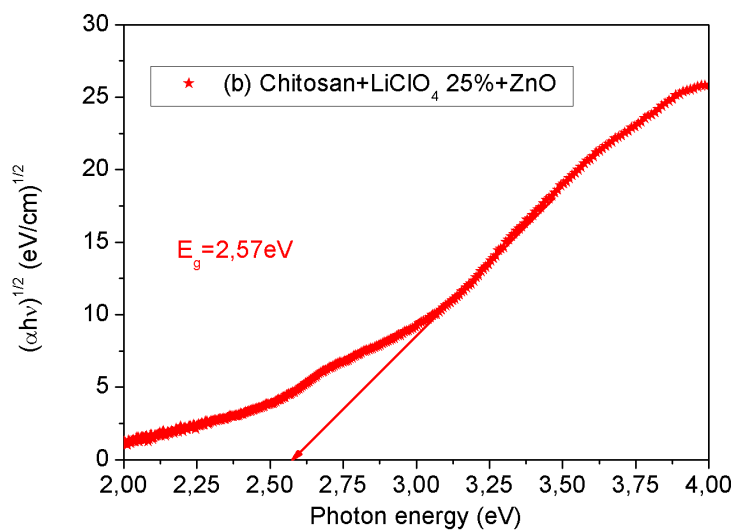
Figure B.7: Tauc plot for band gap of chitosan doped with ZnO and 25% LiClO$_4$
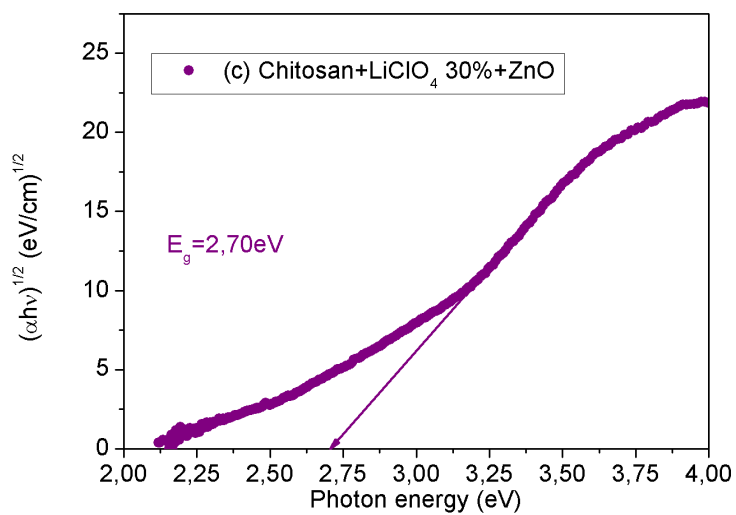
Figure B.8: Tauc plot for band gap of chitosan doped with ZnO and 30% LiClO$_4$
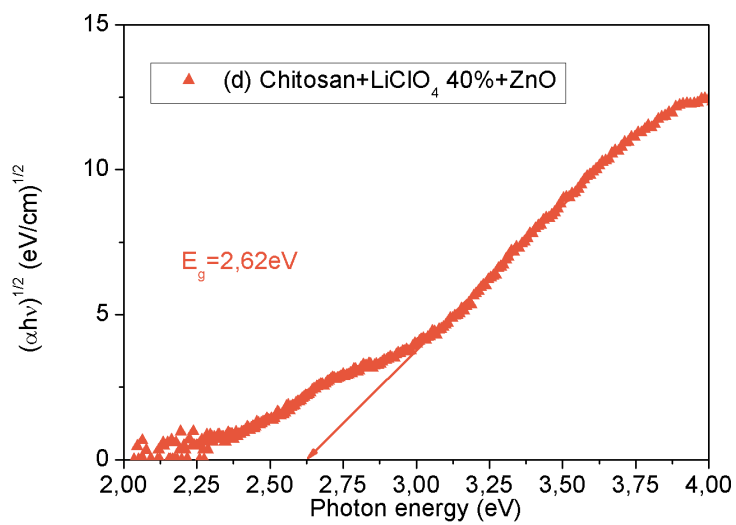
Figure B.9: Tauc plot for band gap of chitosan doped with ZnO and 40% LiClO$_4$

Bibliography

[1] Ng, L.; Mohamad, A. Protonic battery based on a plasticized chitosan-NH4NO3 solid polymer electrolyte. *Journal of Power Sources* **2006**, *163*, 382–385.

[2] Taib, N. U.; Idris, N. H. Plastic crystal–solid biopolymer electrolytes for rechargeable lithium batteries. *Journal of membrane science* **2014**, *468*, 149–154.

[3] Morni, N.; Arof, A. Chitosan–lithium triflate electrolyte in secondary lithium cells. *Journal of power sources* **1999**, *77*, 42–48.

[4] Sudhakar, Y.; Selvakumar, M. Lithium perchlorate doped plasticized chitosan and starch blend as biodegradable polymer electrolyte for supercapacitors. *Electrochimica acta* **2012**, *78*, 398–405.

[5] Ma, J.; Sahai, Y. Chitosan biopolymer for fuel cell applications. *Carbohydrate Polymers* **2013**, *92*, 955–975.

[6] Jürgensen, N.; Zimmermann, J.; Morfa, A. J.; Hernandez-Sosa, G. Biodegradable polycaprolactone as ion solvating polymer for solution-processed light-emitting electrochemical cells. *Scientific reports* **2016**, *6*, 36643.

[7] Ngai, K. S.; Ramesh, S.; Ramesh, K.; Juan, J. C. A review of polymer electrolytes: fundamental, approaches and applications. *Ionics* **2016**, *22*, 1259–1279.

[8] Bruce, P. G.; Scrosati, B.; Tarascon, J.-M. Nanomaterials for rechargeable lithium batteries. *Angewandte Chemie International Edition* **2008**, *47*, 2930–2946.

[9] Maier, J. *Materials For Sustainable Energy: A Collection of Peer-Reviewed Research and Review Articles from Nature Publishing Group*; World Scientific, 2011; pp 160–170.

[10] Arya, A.; Sharma, A. Polymer electrolytes for lithium ion batteries: a critical study. *Ionics* **2017**, *23*, 497–540.

[11] Mainar, A. R.; Iruin, E.; Colmenares, L. C.; Kvasha, A.; de Meatza, I.; Bengoechea, M.; Leonet, O.; Boyano, I.; Zhang, Z.; Blazquez, J. A. An overview of progress in electrolytes for secondary zinc-air batteries and other storage systems based on zinc. *Journal of Energy Storage* **2018**, *15*, 304–328.

[12] Gupta, S.; Singh, P. K.; Bhattacharya, B. Low-viscosity ionic liquid–doped solid polymer electrolytes: Electrical, dielectric, and ion transport studies. *High Performance Polymers* **2018**, *30*, 986–992.

[13] Li, Q.; Aili, D.; Hjuler, H. A.; Jensen, J. O. High temperature polymer electrolyte membrane fuel cells. *Springer, Switzerland* **2016**,

[14] Ue, M.; Takeda, M.; Toriumi, A.; Kominato, A.; Hagiwara, R.; Ito, Y. Application of low-viscosity ionic liquid to the electrolyte of double-layer capacitors. *Journal of the Electrochemical Society* **2003**, *150*, A499–A502.

[15] Sato, T.; Maruo, T.; Marukane, S.; Takagi, K. Ionic liquids containing carbonate solvent as electrolytes for lithium ion cells. *Journal of Power Sources* **2004**, *138*, 253–261.

[16] Capiglia, C.; Mustarelli, P.; Quartarone, E.; Tomasi, C.; Magistris, A. Effects of nanoscale SiO2 on the thermal and transport properties of solvent-free, poly (ethylene oxide)(PEO)-based polymer electrolytes. *Solid state ionics* **1999**, *118*, 73–79.

[17] Teoh, K.; Ramesh, S.; Arof, A. Investigation on the effect of nanosilica towards corn starch–lithium perchlorate-based polymer electrolytes. *Journal of Solid State Electrochemistry* **2012**, *16*, 3165–3170.

[18] Rajendran, S.; Mahendran, O.; Kannan, R. Ionic conductivity studies in composite solid polymer electrolytes based on methylmethacrylate. *Journal of Physics and Chemistry of Solids* **2002**, *63*, 303–307.

[19] Ramesh, S.; Yin, T. S.; Liew, C.-W. Effect of dibutyl phthalate as plasticizer on high-molecular weight poly (vinyl chloride)–lithium tetraborate-based solid polymer electrolytes. *Ionics* **2011**, *17*, 705.

[20] Liew, C.-W.; Ramesh, S.; Ramesh, K.; Arof, A. Preparation and characterization of lithium ion conducting ionic liquid-based biodegradable corn starch polymer electrolytes. *Journal of Solid State Electrochemistry* **2012**, *16*, 1869–1875.

[21] Ramesh, S.; Wen, L. C. Investigation on the effects of addition of SiO 2 nanoparticles on ionic conductivity, FTIR, and thermal properties of nanocomposite PMMA–LiCF 3 SO 3–SiO 2. *Ionics* **2010**, *16*, 255–262.

[22] Alves, R.; Sentanin, F.; Sabadini, R.; Pawlicka, A.; Silva, M. M. Green polymer electrolytes of chitosan doped with erbium triflate. *Journal of Non-Crystalline Solids* **2018**, *482*, 183–191.

[23] Molinaro, G.; Leroux, J.-C.; Damas, J.; Adam, A. Biocompatibility of thermosensitive chitosan-based hydrogels: an in vivo experimental approach to injectable biomaterials. *Biomaterials* **2002**, *23*, 2717–2722.

[24] Wang, X.; Du, Y.; Liu, H. Preparation, characterization and antimicrobial activity of chitosan–Zn complex. *Carbohydrate polymers* **2004**, *56*, 21–26.

[25] Olatunji, O. *Natural Polymers*; Springer, 2016; pp 1–17.

[26] Rinaudo, M. Chitin and chitosan: properties and applications. *Progress in polymer science* **2006**, *31*, 603–632.

[27] Wang, J.; Chen, C. Chitosan-based biosorbents: modification and application for biosorption of heavy metals and radionuclides. *Bioresource technology* **2014**, *160*, 129–141.

[28] Krajewska, B. Diffusional properties of chitosan hydrogel membranes. *Journal of Chemical Technology & Biotechnology: International Research in Process, Environmental & Clean Technology* **2001**, *76*, 636–642.

[29] Aziz, S. B.; Abidin, Z. H. Z.; Kadir, M. Innovative method to avoid the reduction of silver ions to silver nanoparticles in silver ion conducting based polymer electrolytes. *Physica Scripta* **2015**, *90*, 035808.

[30] Kyzas, G. Z.; Bikiaris, D. N. Recent modifications of chitosan for adsorption applications: a critical and systematic review. *Marine drugs* **2015**, *13*, 312–337.

[31] Liu, L.; Sun, G. Promoting the OH-Ion Conductivity of Chitosan Membrane Using Quaternary Phosphonium Polymer Brush Functionalized Graphene Oxide. *INTERNATIONAL JOURNAL OF ELECTROCHEMICAL SCIENCE* **2017**, *12*, 9262–9278.

[32] Hosseini, N. R.; Lee, J.-S. Biocompatible and Flexible Chitosan-Based Resistive Switching Memory with Magnesium Electrodes. *Advanced Functional Materials* **2015**, *25*, 5586–5592.

[33] Kumar, M. N. R. A review of chitin and chitosan applications. *Reactive and functional polymers* **2000**, *46*, 1–27.

[34] Khiar, A.; Puteh, R.; Arof, A. Conductivity studies of a chitosan-based polymer electrolyte. *Physica B: Condensed Matter* **2006**, *373*, 23–27.

[35] Morni, N.; Mohamed, N.; Arof, A. Silver nitrate doped chitosan acetate films and electrochemical cell performance. *Materials Science and Engineering: B* **1997**, *45*, 140–146.

[36] Wan, Y.; Creber, K. A.; Peppley, B.; Bui, V. T. Ionic conductivity of chitosan membranes. *Polymer* **2003**, *44*, 1057–1065.

[37] Yang, R.; Li, H.; Huang, M.; Yang, H.; Li, A. A review on chitosan-based flocculants and their applications in water treatment. *Water research* **2016**, *95*, 59–89.

[38] Wan, Y.; Creber, K. A.; Peppley, B.; Bui, V. T. Chitosan-based electrolyte composite membranes: II. Mechanical properties and ionic conductivity. *Journal of Membrane Science* **2006**, *284*, 331–338.

[39] Du, J.; Bai, Y.; Chu, W.; Qiao, L. Synthesis and performance of proton conducting chitosan/NH4Cl electrolyte. *Journal of Polymer Science Part B: Polymer Physics* **2010**, *48*, 260–266.

[40] Wan, Y.; Creber, K. A.; Peppley, B.; Bui, V. T. Synthesis, characterization and ionic conductive properties of phosphorylated chitosan membranes. *Macromolecular Chemistry and Physics* **2003**, *204*, 850–858.

[41] Soontarapa, K.; Intra, U. Chitosan-based fuel cell membranes. *Chemical Engineering Communications* **2006**, *193*, 855–868.

[42] Mohamed, N.; Subban, R.; Arof, A. Polymer batteries fabricated from lithium complexed acetylated chitosan. *Journal of Power Sources* **1995**, *56*, 153–156.

[43] Fauzi, I.; Arcana, I.; Wahyuningrum, D. Synthesis and Characterization of Solid Polymer Electrolyte from N-Succinyl Chitosan and Lithium Perchlorate. **2014**, *896*, 58–61.

[44] Murthy, K.; Virk, H. S. Luminescence phenomena: An introduction. Defect and Diffusion Forum. 2014; pp 1–34.

[45] Fernandes, D.; Hechenleitner, A. W.; Lima, S.; Andrade, L.; Caires, A.; Pineda, E. G. Preparation, characterization, and photoluminescence study of PVA/ZnO nanocomposite films. *Materials Chemistry and Physics* **2011**, *128*, 371–376.

[46] Feng, Y.; Xu, H. Y.; Nie, W. Y.; Ying, J. Y. Synthesis and characterization of luminescent organic-inorganic hybrid nanocomposite from polyhedral oligomeric silsesquioxane. *Chinese Chemical Letters* **2010**, *21*, 753–757.

[47] Khanna, P.; Singh, N. Light emitting CdS quantum dots in PMMA: synthesis and optical studies. *Journal of Luminescence* **2007**, *127*, 474–482.

[48] Liu, J.-g.; Liang, J.-g.; Han, H.-y.; Sheng, Z.-h. Facile synthesis and characterization of CdTe quantum dots–polystyrene fluorescent composite nanospheres. *Materials Letters* **2009**, *63*, 2224–2226.

[49] Ambika, S.; Sundrarajan, M. Antibacterial behaviour of Vitex negundo extract assisted ZnO nanoparticles against pathogenic bacteria. *Journal of photochemistry and photobiology B: biology* **2015**, *146*, 52–57.

[50] Svetlichnyi, V.; Shabalina, A.; Lapin, I.; Goncharova, D.; Nemoykina, A. ZnO nanoparticles obtained by pulsed laser ablation and their composite with cotton fabric: Preparation and study of antibacterial activity. *Applied Surface Science* **2016**, *372*, 20–29.

[51] Zhang, Z.-Y.; Xiong, H.-M. Photoluminescent ZnO nanoparticles and their biological applications. *Materials* **2015**, *8*, 3101–3127.

[52] Raji, R.; Gopchandran, K. ZnO nanostructures with tunable visible luminescence: effects of kinetics of chemical reduction and annealing. *Journal of Science: Advanced Materials and Devices* **2017**, *2*, 51–58.

[53] Kohan, A.; Ceder, G.; Morgan, D.; Van de Walle, C. G. First-principles study of native point defects in ZnO. *Physical Review B* **2000**, *61*, 15019.

[54] Guo, B.; Qiu, Z.; Wong, K. Intensity dependence and transient dynamics of donor–acceptor pair recombination in ZnO thin films grown on (001) silicon. *Applied physics letters* **2003**, *82*, 2290–2292.

[55] Leiter, F.; Alves, H.; Hofstaetter, A.; Hofmann, D.; Meyer, B. The oxygen vacancy as the origin of a green emission in undoped ZnO. *physica status solidi (b)* **2001**, *226*, R4–R5.

[56] Leiter, F.; Alves, H.; Pfisterer, D.; Romanov, N.; Hofmann, D.; Meyer, B. Oxygen vacancies in ZnO. *Physica B: Condensed Matter* **2003**, *340*, 201–204.

[57] Shan, F.; Liu, G.; Lee, W.; Lee, G.; Kim, I.; Shin, B. Aging effect and origin of deep-level emission in ZnO thin film deposited by pulsed laser deposition. *Applied Physics Letters* **2005**, *86*, 221910.

[58] Liu, M.; Kitai, A.; Mascher, P. Point defects and luminescence centres in zinc oxide and zinc oxide doped with manganese. *Journal of Luminescence* **1992**, *54*, 35–42.

[59] Reynolds, D.; Look, D. C.; Jogai, B.; Hoelscher, J.; Sherriff, R.; Harris, M.; Callahan, M. Time-resolved photoluminescence lifetime measurements of the Γ 5 and Γ 6 free excitons in ZnO. *Journal of Applied Physics* **2000**, *88*, 2152–2153.

[60] Özgür, Ü.; Alivov, Y. I.; Liu, C.; Teke, A.; Reshchikov, M.; Doğan, S.; Avrutin, V.; Cho, S.-J.; Morkoç, H. A comprehensive review of ZnO materials and devices. *Journal of applied physics* **2005**, *98*, 11.

[61] Pal, U.; Serrano, J. G.; Santiago, P.; Xiong, G.; Ucer, K.; Williams, R. Synthesis and optical properties of ZnO nanostructures with different morphologies. *Optical Materials* **2006**, *29*, 65–69.

[62] Janotti, A.; Van de Walle, C. G. Fundamentals of zinc oxide as a semiconductor. *Reports on progress in physics* **2009**, *72*, 126501.

[63] Lin, O. H.; Akil, H. M.; Mahmud, S. Effect of particle morphology on the properties of polypropylene/nanometric zinc oxide (pp/nanozno) composites. *Advanced Composites Letters* **2009**, *18*, 096369350901800302.

[64] Rayerfrancis, A.; Bhargav, P. B.; Ahmed, N.; Chandra, B.; Dhara, S. Effect of pH on the morphology of ZnO nanostructures and its influence on structural and optical properties. *Physica B: Condensed Matter* **2015**, *457*, 96–102.

[65] Chithra, M. J.; Sathya, M.; Pushpanathan, K. Effect of pH on crystal size and photoluminescence property of ZnO nanoparticles prepared by chemical precipitation method. *Acta Metallurgica Sinica (English Letters)* **2015**, *28*, 394–404.

[66] Oliveira, R. S.; Maia, D. O.; Pereira, M. R.; E Silva, F. R. Preparation, Characterization and Luminescence Study of Chitosan Membrane and Powder Forms with Eu3+ and Tb3+. *Journal of Macromolecular Science, Part A: Pure and Applied Chemistry* **2010**, *47*, 392–398.

[67] Huang, H.; Liu, F.; Chen, S.; Zhao, Q.; Liao, B.; Long, Y.; Zeng, Y.; Xia, X. Enhanced fluorescence of chitosan based on size change of micelles and application to directly selective detecting Fe3+ in humanserum. *Biosensors and Bioelectronics* **2013**, *42*, 539–544.

[68] Pan, X.; Ren, W.; Gu, L.; Wang, G.; Liu, Y. Photoluminescence from chitosan for bio-imaging. *Australian Journal of Chemistry* **2014**, *67*, 1422–1426.

[69] Marpu, S.; Benton, E. Shining light on chitosan: A review on the usage of chitosan for photonics and nanomaterials research. *International journal of molecular sciences* **2018**, *19*, 1795.

[70] Tsvirko, M.; Mandowska, E.; Biernacka, M.; Tkaczyk, S.; Mandowski, A. Luminescence properties of chitosan doped with europium complex. *Journal of Luminescence* **2013**, *143*, 128–131.

[71] Alves, R.; Ravaro, L. P.; Pawlicka, A.; Silva, M. M.; de Camargo, A. S. Eco-friendly luminescent hybrid materials based on EuIII and LiI co-doped chitosan. *Journal of the Brazilian Chemical Society* **2015**, *26*, 2590–2597.

[72] Alves, R.; De Camargo, A.; Pawlicka, A.; Silva, M. M. Luminescent polymer electrolytes based on chitosan and containing europium triflate. *Journal of Rare Earths* **2016**, *34*, 661–666.

[73] Postek, M. T.; Howard, K. S.; Johnson, A. H.; McMichael, K. L. The scanning electron microscope. *Handbook of charged particle optics* **1997**, 363–399.

[74] Zhou, W.; Wang, Z. L. *Scanning microscopy for nanotechnology: techniques and applications*; Springer science & business media, 2007.

[75] Holt, D. B.; Joy, D. C. *SEM microcharacterization of semiconductors*; Academic Press, 2013; Vol. 12.

[76] Bates, J. Fourier transform infrared spectroscopy. *Science* **1976**, *191*, 31–37.

[77] Siesler, H. W.; Ozaki, Y.; Kawata, S.; Heise, H. M. *Near-infrared spectroscopy: principles, instruments, applications*; John Wiley & Sons, 2008.

[78] Harris, D. C.; Bertolucci, M. D. *Symmetry and spectroscopy: an introduction to vibrational and electronic spectroscopy*; Courier Corporation, 1989.

[79] Theophile, T. *Infrared spectroscopy: Materials science, engineering and technology*; BoD–Books on Demand, 2012.

[80] Berthomieu, C.; Hienerwadel, R. Fourier transform infrared (FTIR) spectroscopy. *Photosynthesis research* **2009**, *101*, 157–170.

[81] Epp, J. *Materials characterization using Nondestructive Evaluation (NDE) methods*; Elsevier, 2016; pp 81–124.

[82] others,, *et al. Structure determination from powder diffraction data*; Oxford University Press on Demand, 2002; Vol. 13.

[83] Igwebike-Ossi, C. D. *Failure Analysis and Prevention*; IntechOpen, 2017.

[84] Bunaciu, A. A.; UdriŞTioiu, E. G.; Aboul-Enein, H. Y. X-ray diffraction: instrumentation and applications. *Critical Reviews in Analytical Chemistry* **2015**, *45*, 289–299.

[85] Cottis, R.; Turgoose, S. *Electrochemical impedance and noise*; National Assn of Corrosion Engineers, 1999; Vol. 7.

[86] Ahmad, Z. *Principles of corrosion engineering and corrosion control*; Elsevier, 2006.

[87] Lvovich, V. F. *Impedance spectroscopy: applications to electrochemical and dielectric phenomena*; John Wiley & Sons, 2012.

[88] Barsoukov, E.; Macdonald, J. R. *Impedance spectroscopy: theory, experiment, and applications*; John Wiley & Sons, 2018.

[89] Retter, U.; Lohse, H. *Electroanalytical Methods*; Springer, 2010; pp 159–177.

[90] Lasia, A. *Modern aspects of electrochemistry*; Springer, 2002; pp 143–248.

[91] Aziz, S. B.; Abdullah, O. G.; Rasheed, M. A.; Ahmed, H. M. Effect of high salt concentration (HSC) on structural, morphological, and electrical characteristics of chitosan based solid polymer electrolytes. *Polymers* **2017**, *9*, 187.

[92] Navaratnam, S.; Ramesh, K.; Ramesh, S.; Sanusi, A.; Basirun, W.; Arof, A. Transport mechanism studies of chitosan electrolyte systems. *Electrochimica Acta* **2015**, *175*, 68–73.

[93] YU, P.; Cardona, M. *Fundamentals of Semiconductors: Physics and Materials Properties*; Advanced texts in physics v. 3; Springer Berlin Heidelberg, 2005.

[94] Martinsen, O. G.; Grimnes, S. *Bioimpedance and bioelectricity basics*; Academic press, 2011.

[95] Kao, K. C. *Dielectric phenomena in solids*; Elsevier, 2004.

[96] Buraidah, M.; Arof, A. Characterization of chitosan/PVA blended electrolyte doped with NH4I. *Journal of Non-Crystalline Solids* **2011**, *357*, 3261–3266.

[97] Aziz, S. B.; Al-Zangana, S.; Woo, H.; Kadir, M.; Abdullah, O. G. The compatibility of chitosan with divalent salts over monovalent salts for the preparation of solid polymer electrolytes. *Results in Physics* **2018**, *11*, 826–836.

[98] Wise, D. L. *Electrical and optical polymer systems: fundamentals: Methods, and applications*; CRC Press, 1998.

[99] Maensiri, S.; Masingboon, C.; Promarak, V.; Seraphin, S. Synthesis and optical properties of nanocrystalline V-doped ZnO powders. *Optical Materials* **2007**, *29*, 1700–1705.

[100] Rathod, S. G.; Bhajantri, R.; Ravindrachary, V.; Pujari, P.; Sheela, T. Ionic conductivity and dielectric studies of LiClO 4 doped poly (vinylalcohol)(PVA)/chitosan (CS) composites. *Journal of Advanced Dielectrics* **2014**, *4*, 1450033.

[101] Yesappa, L.; Niranjana, M.; Ashokkumar, S.; Vijeth, H.; Basappa, M.; Dwivedi, J.; Petwal, V.; Ganesh, S.; Devendrappa, H. Optical properties and ionic conductivity studies of an 8 MeV electron beam irradiated poly (vinylidene fluoride-co-hexafluoropropylene)/LiClO 4 electrolyte film for opto-electronic applications. *RSC Advances* **2018**, *8*, 15297–15309.

[102] Manikandan, K.; Dilip, C. S.; Mani, P.; Prince, J. J. Deposition and characterization of CdS nano thin film with complexing agent triethanolamine. *American Journal of Engineering and Applied Sciences* **2015**, *8*, 318.

[103] Magesh, G.; Bhoopathi, G.; Nithya, N.; Arun, A.; Kumar, E. R. Tuning effect of polysaccharide Chitosan on structural, morphological, optical and photoluminescence properties of ZnO nanoparticles. *Superlattices and Microstructures* **2018**, *117*, 36–45.

[104] Carlos, L. D.; Palacio, F. *Thermometry at the Nanoscale: Techniques and Selected Applications*; Royal Society of Chemistry, 2015.

[105] Rotman, S. R. *Wide-gap luminescent materials: theory and applications*; Springer, 1997.

[106] Kitai, A. *Luminescent materials and applications*; John Wiley & Sons, 2008; Vol. 25.

[107] Gerrish, V. M. *Semiconductors and Semimetals*; Elsevier, 1995; Vol. 43; pp 493–530.

[108] Ronda, C. R. *Luminescence: from theory to applications*; John Wiley & Sons, 2007.

[109] McKeever, S. W. *Thermoluminescence of solids*; Cambridge University Press, 1988; Vol. 3.

[110] Skoog, D. A.; Holler, F. J.; Crouch, S. R. *Principles of instrumental analysis*; Cengage learning, 2017.

[111] Berezin, M. Y.; Achilefu, S. Fluorescence lifetime measurements and biological imaging. *Chemical reviews* **2010**, *110*, 2641–2684.

[112] Ishikawa-Ankerhold, H. C.; Ankerhold, R.; Drummen, G. P. Advanced fluorescence microscopy techniquesâĂŤFrap, Flip, Flap, Fret and flim. *Molecules* **2012**, *17*, 4047–4132.

[113] Kumar, S.; Koh, J. Physiochemical and optical properties of chitosan based graphene oxide bionanocomposite. *International journal of biological macromolecules* **2014**, *70*, 559–564.

[114] Ishak, K. M. K.; Ahmad, Z.; Akil, H. M. Synthesis and characterization of cis-5-norbornene-2, 3-dicarboxylic anhydride-chitosan. *e-Polymers* **2010**, *10*.

[115] El-Hefian, E. A.; NASEF, M.; Yahaya, A. H.; Khan, R. A. Preparation and characterization of chitosan/agar blends: rheological and thermal studies. *Journal of the Chilean Chemical Society* **2010**, *55*, 130–136.

[116] Mohammad, A. M.; Eldin, T. A. S.; Hassan, M. A.; El-Anadouli, B. E. Efficient treatment of lead-containing wastewater by hydroxyapatite/chitosan nanostructures. *Arabian Journal of Chemistry* **2017**, *10*, 683–690.

[117] Mitra, T.; Sailakshmi, G.; Gnanamani, A.; Mandal, A. Studies on cross-linking of succinic acid with chitosan/collagen. *Materials Research* **2013**, *16*, 755–765.

[118] Alhosseini, S. N.; Moztarzadeh, F.; Mozafari, M.; Asgari, S.; Dodel, M.; Samadikuchaksaraei, A.; Kargozar, S.; Jalali, N. Synthesis and characterization of electrospun polyvinyl alcohol nanofibrous scaffolds modified by blending with chitosan for neural tissue engineering. *International journal of nanomedicine* **2012**, *7*, 25.

[119] Song, C.; Yu, H.; Zhang, M.; Yang, Y.; Zhang, G. Physicochemical properties and antioxidant activity of chitosan from the blowfly Chrysomya megacephala larvae. *International journal of biological macromolecules* **2013**, *60*, 347–354.

[120] AbdElhady, M. Preparation and characterization of chitosan/zinc oxide nanoparticles for imparting antimicrobial and UV protection to cotton fabric. *International journal of carbohydrate chemistry* **2012**, *2012*.

[121] Buşilă, M.; Muşat, V.; Textor, T.; Mahltig, B. Synthesis and characterization of antimicrobial textile finishing based on Ag: ZnO nanoparticles/chitosan biocomposites. *Rsc Advances* **2015**, *5*, 21562–21571.

[122] Khorasani, M. T.; Joorabloo, A.; Moghaddam, A.; Shamsi, H.; MansooriMoghadam, Z. Incorporation of ZnO nanoparticles into heparinised polyvinyl alcohol/chitosan hydrogels for wound dressing application. *International journal of biological macromolecules* **2018**, *114*, 1203–1215.

[123] Abarna, S.; Hirankumar, G. Study on new lithium ion conducting electrolyte based on polyethylene glycol-p-tertoctyl phenyl ether and lithium perchlorate. *Int J ChemTech Res* **2014**, *6*, 5161–5167.

[124] TABOADA, E.; Cabrera, G.; Cardenas, G. Retention capacity of chitosan for copper and mercury ions. *Journal of the Chilean Chemical Society* **2003**, *48*, 7–12.

[125] Kumar, S.; Koh, J. Physiochemical and optical study of chitosan–terephthaldehyde derivative for biomedical applications. *International journal of biological macromolecules* **2012**, *51*, 1167–1172.

[126] Saravanan, A.; Ramasamy, R. P. Chitosan-maghemite-LiClO 4–a new green conducting superpara magnetic nanocomposite. *Journal of Polymer Research* **2016**, *23*, 174.

[127] Yusof, N. A. A.; Zain, N. M.; Pauzi, N. Synthesis of ZnO nanoparticles with chitosan as stabilizing agent and their antibacterial properties against Gram-positive and Gram-negative bacteria. *International journal of biological macromolecules* **2019**, *124*, 1132–1136.

[128] Rahman, P. M.; Mujeeb, V. A.; Muraleedharan, K.; Thomas, S. K. Chitosan/nano ZnO composite films: enhanced mechanical, antimicrobial and dielectric properties. *Arabian Journal of Chemistry* **2018**, *11*, 120–127.

[129] Salman, Y. A.; Abdullah, O. G.; Hanna, R. R.; Aziz, S. B. Conductivity and Electrical Properties of Chitosan-Methylcellulose Blend Biopolymer Electrolyte Incorporated with Lithium Tetrafluoroborate. *INTERNATIONAL JOURNAL OF ELECTROCHEMICAL SCIENCE* **2018**, *13*, 3185–3199.

[130] Aziz, S. B.; Abidin, Z. H. Z. Role of Hard-Acid/Hard-Base Interaction on Structural and Dielectric Behavior of Solid Polymer Electrolytes Based on Chitosan-XCF3SO3 (X= Li. *Journal of Polymers* **2014**, *2014*.

[131] Perumal, P.; Selvin, P. C.; Selvasekarapandian, S.; Sivaraj, P.; Abhilash, K.; Moniha, V.; Devi, R. M. Plasticizer incorporated, novel eco-friendly bio-polymer based solid bio-membrane for electrochemical clean energy applications. *Polymer Degradation and Stability* **2019**, *159*, 43–53.

[132] Fadzallah, I.; Majid, S.; Careem, M.; Arof, A. Relaxation process in chitosan–oxalic acid solid polymer electrolytes. *Ionics* **2014**, *20*, 969–975.

[133] Croisier, F.; Jérôme, C. Chitosan-based biomaterials for tissue engineering. *European Polymer Journal* **2013**, *49*, 780–792.

[134] Wu, G.; Zhang, J.; Wan, X.; Yang, Y.; Jiang, S. Chitosan-based biopolysaccharide proton conductors for synaptic transistors on paper substrates. *Journal of Materials Chemistry C* **2014**, *2*, 6249–6255.

[135] Ahmed, R. A.; Farghali, R.; Fekry, A. Study for the stability and corrosion inhibition of electrophoretic deposited chitosan on mild steel alloy in acidic medium. *International Journal of Electrochemical Science* **2012**, *7*, 7270–7282.

[136] Amador, A. S.; Guerrero-Barajas, S.; Hernandez-Salas, D.; Sierra-Herrera, D.; Estupiñan-Duran, H.; Ballesteros, D. P. In vitro electrochemical behaviour of Chitosan-PEG coatings obtained on Ti6Al4V by dip coating. Journal of Physics: Conference Series. 2017; p 012030.

[137] Rodrigues, I. R.; de Camargo Forte, M. M.; Azambuja, D. S.; Castagno, K. R. Synthesis and characterization of hybrid polymeric networks (HPN) based on polyvinyl alcohol/chitosan. *Reactive and Functional Polymers* **2007**, *67*, 708–715.

[138] Kumar, M. S.; Bhat, D. K. Polyvinyl alcohol–polystyrene sulphonic acid blend electrolyte for supercapacitor application. *Physica B: Condensed Matter* **2009**, *404*, 1143–1147.

[139] Pradhan, D. K.; Choudhary, R.; Samantaray, B. Studies of dielectric relaxation and AC conductivity behavior of plasticized polymer nanocomposite electrolytes. *Int. J. Electrochem. Sci* **2008**, *3*, 597–608.

[140] Qian, X.; Gu, N.; Cheng, Z.; Yang, X.; Wang, E.; Dong, S. Impedance study of (PEO) 10LiClO4–Al2O3 composite polymer electrolyte with blocking electrodes. *Electrochimica acta* **2001**, *46*, 1829–1836.

[141] Govindaraj, G.; Baskaran, N.; Shahi, K.; Monoravi, P. Preparation, conductivity, complex permittivity and electric modulus in AgIîŮÿ Ag2OîŮÿ SeO3îŮÿ MoO3 glasses. *Solid State Ionics* **1995**, *76*, 47–55.

[142] Ramesh, S.; Yahaya, A.; Arof, A. Dielectric behaviour of PVC-based polymer electrolytes. *Solid State Ionics* **2002**, *152*, 291–294.

[143] Ramesh, S.; Arof, A. Structural, thermal and electrochemical cell characteristics of poly (vinyl chloride)-based polymer electrolytes. *Journal of power sources* **2001**, *99*, 41–47.

[144] Aziz, S. B. Study of electrical percolation phenomenon from the dielectric and electric modulus analysis. *Bulletin of Materials Science* **2015**, *38*, 1597–1602.

[145] Sudhakar, Y.; Selvakumar, M.; Bhat, D. K. *Biopolymer Electrolytes: Fundamentals and Applications in Energy Storage*; Elsevier, 2018.

[146] Begum, S.; Pandian, R.; Aswal, V. K.; Ramasamy, R. P. Chitosan–gold–lithium nanocomposites as solid polymer electrolyte. *Journal of nanoscience and nanotechnology* **2014**, *14*, 5761–5773.

[147] Li, L.-H.; Deng, J.-C.; Deng, H.-R.; Liu, Z.-L.; Xin, L. Synthesis and characterization of chitosan/ZnO nanoparticle composite membranes. *Carbohydrate Research* **2010**, *345*, 994–998.

[148] Vaseeharan, B.; Sivakamavalli, J.; Thaya, R. Synthesis and characterization of chitosan-ZnO composite and its antibiofilm activity against aquatic bacteria. *Journal of Composite Materials* **2015**, *49*, 177–184.

[149] Fooladsaz, K.; Negahdary, M.; Rahimi, G.; Habibi-Tamijani, A.; Parsania, S.; Akbari-dastjerdi, H.; Sayad, A.; Jamaleddini, A.; Salahi, F.; Asadi, A. Dopamine determination with a biosensor based on catalase and modified carbon paste electrode with zinc oxide nanoparticles. *Int. J. Electrochem. Sci* **2012**, *7*, 9892–9908.

[150] Arefi, M. R.; Rezaei-Zarchi, S. Synthesis of zinc oxide nanoparticles and their effect on the compressive strength and setting time of self-compacted concrete paste as cementitious composites. *International journal of molecular sciences* **2012**, *13*, 4340–4350.

[151] Harrison, P.; Valavanis, A. *Quantum wells, wires and dots: theoretical and computational physics of semiconductor nanostructures*; John Wiley & Sons, 2016.

[152] Becheri, A.; Dürr, M.; Nostro, P. L.; Baglioni, P. Synthesis and characterization of zinc oxide nanoparticles: application to textiles as UV-absorbers. *Journal of Nanoparticle Research* **2008**, *10*, 679–689.

[153] Saravanan, R.; Aviles, J.; Gracia, F.; Mosquera, E.; Gupta, V. K. Crystallinity and lowering band gap induced visible light photocatalytic activity of TiO2/CS (Chitosan) nanocomposites. *International journal of biological macromolecules* **2018**, *109*, 1239–1245.

[154] Bakr, N. A.; Khodair, Z. T.; Shano, A. M. Effect of Aqueous Solution Molarity on Structural and Optical Properties of Ni0. 92Co0. 08O Thin Films Prepared by Chemical Spray Pyrolysis Method. *Int. J. Thin. Fil. Sci. Tec* **2015**, *4*, 111–119.

[155] Silva, S. S.; Ferreira, R. A.; Fu, L.; Carlos, L. D.; Mano, J. F.; Reis, R. L.; Rocha, J. Functional nanostructured chitosan–siloxane hybrids. *Journal of Materials Chemistry* **2005**, *15*, 3952–3961.

[156] Meier, S. B.; Tordera, D.; Pertegas, A.; Roldan-Carmona, C.; Ortí, E.; Bolink, H. J. Light-emitting electrochemical cells: recent progress and future prospects. *Materials Today* **2014**, *17*, 217–223.